DØ NOTE 3308
October 3, 1997
V3.6

DØ Optimized Search for First Generation Leptoquarks in the $e\nu jj$ Channel with Run I Data

P. Bhat, S. Hagopian J. Hobbs, D. Karmgard, B. Knuteson,
G. Landsberg, H. Prosper, M. Strovink, G. Wang, G. Watts

ABSTRACT

We have performed an optimized search for first generation leptoquarks in the $e\nu jj$ final state using the entire Run 1 (1992–1996) data corresponding to an integrated luminosity of 115 pb^{-1}, collected with the DØ detector at the Fermilab Tevatron. We find no evidence for leptoquarks in the data. No events remain in the data sample after applying optimized cuts with an expected background of approximately 0.4 events. We also do not see any kinematically interesting events for looser cuts. The analysis yields a 95% C.L. upper limit on the leptoquark production cross section of 0.17 pb at $M_{\rm LQ} = 180$ GeV/c^2. By comparing with the lower band of the NLO theoretical calculations of the leptoquark pair production cross section the 95% CL lower limit on the first generation leptoquark mass of 175 GeV/c^2 is found for the assumption of the leptoquark decay branching ratio (β) to charge lepton being equal to 1/2. Combining with the lower limit on the LQ mass of 175 GeV/c^2 for β=1/2 from an analysis of the $eejj$ final state, we obtain a 95% CL lower limit mass of 204 GeV/c^2. The result of this analysis, together with the previous $eejj$ results make an explanation of HERA data with scalar first generation leptoquark extremely improbable.*

I. INTRODUCTION

This Note describes a new search for leptoquarks (LQ) optimized for the value of the branching ratio of the LQ decay in the charged channel $\beta = 1/2$. We used the $e\nu jj$ final state for this analysis.

Both the logic and the major optimization techniques and tools were developed in the course of the $\beta = 1$ analysis in the $eejj$ channel which was just submitted for publication [1]. The $eejj$ analysis is described in detail in Ref. [2], so this Note will refer to the $eejj$ documentation where possible.

---

*Since some of us hate the DØ convention of using GeV/c, GeV/c^2 dimensions for momenta and masses, since we are used to "natural" $\hbar = c = 1$ system of units, the DØ standard notation is used only in the abstract and in a few figures prepared for the PRL paper.

The interest to explore $\beta < 1$ is suggested by recent theoretical papers [3,4] considering certain ways to get around the $\beta = 1$ restriction strongly favored by HERA data [5] in a broad variety of "conventional" LQ models (see, e.g., discussion in Ref. [6]).

The $eejj$ channel is also sensitive to $\beta < 1$. However, since both LQ's have to decay in the charged mode, the cross section of the LQ pair production in the $eejj$ channel is suppressed by a factor of β^2. The cross section in the $e\nu jj$ channel has a suppression of $2\beta(1-\beta)$, which is smaller at low values of β. Therefore, study of the $e\nu jj$ channel allows to push the LQ mass limit to higher masses for $\beta < 1$.

II. SUMMARY OF PAST DØ FIRST GENERATION LEPTOQUARK RESULTS

DØ has presented preliminary results of the analysis in the $e\nu jj$ channel both at winter conferences [7] and at the HCP'97 this summer [8]. The latest result which reflects an attempt to optimize the analysis by taking into account mass variables of the event resulted in the 95% CL lower limit of 154 GeV for $\beta = 1/2$.

The $eejj$ analysis optimized for $\beta = 1$ also yielded a strong 95% CL lower limit of 175 GeV for $\beta = 1/2$. Combined limits from the above two analysis correspond to $M_{LQ} > 192$ GeV at 95% CL for $\beta = 1/2$.

The new full-fledged optimization takes advantage of the neural net and random grid search methods of optimal cut selection and follows the same strategy: very loose initial cuts and thorough multivariate optimization of the signal against the background.

III. DATA SAMPLES

The entire available data of Tevatron Run I were used in this analysis. Trigger definitions and their integrated luminosities are listed in Table I. Total integrated luminosity of the sample was 115 ± 6 pb^{-1}.

Offline selection required an EM object to have a matching track usable for revertexing (see [2] for details on this technique). The kinematic properties of all the objects (electrons, jets, etc) in the event (such as transverse energies, pseudorapidities, polar angles, etc.) were then recalculated based on the new vertex. In what follows we use these new kinematic quantities to define all the subsequent cuts.

The optimized $e\nu jj$ event selection was done as follows. We started with a very loose sample of the events with one EM cluster and missing energy (Run IB,IC) or a jet (Run IC) selected by the triggers designed for the W (1A,B) or top (1C) selection (see Table I). These events were reconstructed by a standard DØ reconstruction program (DØRECO, v11.17 through v12.21) and streamed in the microDST format [9]. Jet energies and missing transverse energy were corrected using CAFIX v5.0 [10]. Trigger and electron identification efficiency computations are described below. The starting sample contained 95,383 events.

We required one EM cluster with $E_T^{\rm EM} > 20$ GeV and a tight matching track ($\sigma < 10$) in the event, a significant amount of missing transverse energy ($\not{E}_T > 20$ GeV) and in addition at least two jets reconstructed with the $R = 0.7$ cone algorithm with $E_T^j > 20$ GeV. The EM cluster was required to be in a good fiducial volume of the detector, i.e. $|\eta_d^{\rm EM}| < 1.1$ (CC) or $1.5 < |\eta_d^{\rm EM}| < 2.5$ (EC). Jets were required to be within $|\eta^j| < 2.5$. (For fiducial cut definition, pseudorapidity η_d is defined in the detector reference frame, i.e. with $z = 0$ at the center of the detector.) Jets were required to have the electromagnetic fraction (EMF) < 0.95. In the events with any EM cluster with $E_T > 20$ GeV close to a jet ($\Delta R_{\rm min}(\mathrm{EM}-j) < 0.6$) the electron was "subtracted" from the jet in order not to double count the energy in the event. Finally, since the missing transverse energy cut for this analysis was very high (see below) we have chosen to use a "minimal" main ring veto in order to increase signal efficiency: CAL_RECOVERY & GOOD_BEAM = 0. We have also removed "bad" runs with known DAQ/calorimeter problems. We have identified and additionally removed 20 runs during which the calorimeter had a hot cell which resulted in a completely wrong $\not\!\!E_T$ calculation (see Section VII B for details. The above selection resulted in 8,925 events (see Table II).

Similar to the $eejj$ analysis, we used the 5-variable electron likelihood [11] and selected "good" electron by requiring the likelihood to be less than 1.0. Additionally we required electrons to have significant fraction of EM energy (EMF > 0.9) and good energy isolation:

$$\mathrm{ISO} \equiv \frac{(E_{tot}(R=0.4) - E_{\rm EM}(R=0.2))}{E_{\rm EM}(R=0.2)} < 0.15$$

(here $E_{\rm tot}(R = 0.4)$ and $E_{\rm EM}(R = 0.2)$ are the total and EM energies in the $R = 0.4$ or 0.2 cone centered on the EM cluster.

After such a preselection the dominant background in the data sample is from $W + 2j$ events, and, in order to reduce it as well as the QCD background, additional cuts on the $\not\!\!E_T$ and the transverse electron-neutrino mass $M_T^{e\nu}$ were introduced. We required $\not\!\!E_T > 30$ GeV and we also required $\not\!\!E_T$ vector to be isolated from the jets in transverse plane in case when the $\not\!\!E_T$ is not very high. The following simple $\not\!\!E_T$ isolation cut was used:

$$\min(\Delta\phi_{j\not\,E_T}) < 0.25 \text{ for } \not\!\!E_T < 120 \text{ GeV}$$

The effect of the above cut on the QCD background and LQ signal is illustrated by Fig. 1. For the background plot the dots correspond to background before the $M_T^{e\nu}$ cut, and boxes - after it. The cut is 91% efficient for the LQ signal with $M_{LQ} = 180$ GeV. (This efficiency is much higher (97%) for the neural net cuts used in the analysis (see Section VIII).) It is essential for keeping the QCD background low. We have also performed a formal optimization of the cut contour in the ($\min\Delta\phi_{j\not\,E_T}$, $\not\!\!E_T$)-plane and found that the box cut discussed above has approximately the same efficiency as a more elaborate network contour.

A random grid search optimization of the $\not\!\!E_T$ and $M_T^{e\nu}$ variables (see [2] for details on this method) suggested the following cuts:

$$\not\!\!E_T > 30 \text{ GeV}, \quad M_T^{e\nu} > 110 \text{ GeV}.$$

Finally, in order to initially suppress the other major background — from the top quark pair production — we applied a muon veto to the event by requiring no reconstructed muons which pass standard quality cuts used in the $t\bar{t} \to e\mu$ analysis [12]. (These cuts are essentially requirements of the no A-layer stub, calorimeter confirmation and good muon track fit quality.)

These final cuts reduced our base sample to 14 events (see Table II for selection details).

IV. ADDITIONAL VARIABLES

In addition to the E_T's of the electron and jets and $\not{E}_T$ and dM/M used in the previous $e\nu jj$ analysis [13], several new types of variables were explored to improve the efficiency of separating signal from background. These include energy sum variables, invariant mass variables and mass difference variables as listed below.
Energy and Transverse Energy Sums

H_T^L - sum of the E_T's of the two leptons (electron and $\not{E}_T$)
H_T^j - sum of the E_T's of all the jets with $E_T>$ 20 GeV and rapidity $|\eta_d^j| < 2.5$
H_T^{j12} - sum of the E_T's of the two leading (in E_T) jets
H_T^{j123} - sum of the E_T's of the three leading (in E_T) jets
$S_T = H_T^L + H_T^j$ - total sum of objects E_T for the event
$S_T^{12} = H_T^L + H_T^{j12}$ - total sum of the E_T's of the two leading jets and two leptons in the event
S - total energy of the event

Invariant mass variables

$M_T^{e\nu}$ - transverse electron-neutrino mass
M_{ej_1} - invariant mass of electron 1 and jet 1
M_{ej_2} - invariant mass of electron 1 and jet 2
$M_T^{\nu j_1}$ - transverse mass of the neutrino and jet 1
$M_T^{\nu j_2}$ - transverse mass of the neutrino and jet 2

Mass Difference Variables

$$dM/M(120) = min(\frac{abs(M_{ej1}-120)}{120}, \frac{abs(M_{ej2}-120)}{120})$$
$$dM/M(140) = min(\frac{abs(M_{ej1}-140)}{140}, \frac{abs(M_{ej2}-140)}{140})$$
$$dM/M(160) = min(\frac{abs(M_{ej1}-160)}{160}, \frac{abs(M_{ej2}-160)}{160})$$
$$dM/M(180) = min(\frac{abs(M_{ej1}-180)}{180}, \frac{abs(M_{ej2}-180)}{180})$$
$$dM/M(200) = min(\frac{abs(M_{ej1}-200)}{200}, \frac{abs(M_{ej2}-200)}{200})$$

where M_{ej1} and M_{ej2} are the invariant masses of the electron with the first and the second jet respectively.

These variables were tried in various combinations in the cut optimizations studies. We found S_T^{12} and $dM/M(180)$ to be the most powerful variables for optimizing the sensitivity for $\beta = 1/2$ LQ. For other values of β we found that changing the dM/M mass scale gives an improvement (see Section VIII for details).

V. SIGNAL AND BACKGROUND SAMPLES

A. LQ Monte Carlo Samples

We used ISAJET v7.21 event generator followed by the full detector simulation via GEANT [14] with shower library to model the LQ signal. Two to five thousand events were generated for each LQ mass point between 100 and 220 GeV in 20 GeV steps. We have also used PYTHIA [15] MC sample for the LQ mass of 200 GeV to facilitate MC systematics studies and various cross checks. The signal MC statistics used in this analysis as well as the NLO pair production cross sections [16] are summarized in Table III.

B. $W + 2j$ Monte Carlo Sample

We used the top group VECBOS [17] $W + 2j$ sample followed by the ISAJET underlying event modeling and GEANT detector simulation in order to study the $W + 2j$ background. This sample contains 227,726 events and corresponds to an integrated luminosity of 0.8 fb^{-1}.

As it turned out (see Section VII C), such statistics are marginally sufficient to get the background estimates. A possibility to generate additional events to decrease an error on the background is under study.

C. $t\bar{t}$ Monte Carlo Sample

The $t\bar{t}\rightarrow$ lepton+jets and dilepton+jets Monte Carlo sample was produced by the top group using HERWIG [18] for $m_t = 170$ GeV followed by GEANT detector simulation. It contains 81,141 events corresponding to an integrated luminosity of about 32 fb^{-1} (taking into account total branching ratio into lepton+jets and dileptons+jets of 45.6% and the measured DØ top cross section of 5.7 ± 1.8 pb [19]).

D. QCD Data Sets for Background Studies

The QCD background was estimated using the run IB data taken with the JET_3_MON trigger which required three jets with $E_T^j > 10$ GeV at Level 2. This trigger was prescaled and had the integrated luminosity of 0.936 pb^{-1}. The QCD mini-stream which required at least two jets with $E_T^j > 15$ GeV and at least one additional jet with $E_T^j > 20$ GeV was produced from this trigger. It contained 356,415 events.

VI. EFFICIENCIES

A. Trigger Efficiency

Trigger requirements are very efficient since the base sample has a high cut on both the EM cluster and missing transverse energies. The turn-on curve for the EM part of the trigger has been already studied in [2]. It gives essentially 100% efficiency for Run Ia trigger and (99.5 ± 0.5)% efficiency for Run IB trigger, since the $\not{E}_T$ cut is in the trigger plateau region.

The efficiency for Run IC trigger that has a jet requirement was estimated by comparing jet energy spectra in $W + 2j$ events collected with Run IA and Run IC triggers. It turned out that trigger starts to be efficient at about 20 GeV and is fully efficient above 30 GeV (in agreement with the QCD trigger rule of thumb: offline plateau starts at twice the L2 threshold). Since the LQ signal has a high probability of at least one jet to have transverse energy above 30 GeV, folding the turn-on curve with the LQ signal distribution gives an efficiency of (99 ± 1)% for this part of the run for the LQ mass range within the scope of this analysis. Overall the trigger efficiency is (99.5 ± 0.5)%.

B. Active Veto Efficiency

The efficiency of the active veto requirement (CAL_RECOVERY & GOOD_BEAM = 0) was estimated using $Z + 2j$ data set. Since the Z triggers (see Ref. [2]) have a looser active veto requirement than the triggers used in this analysis, first the $e\nu jj$ data set active veto requirement was introduced and then the efficiency was calculated by counting the loss of the event in the Z-peak after the additional (CAL_RECOVERY& GOOD_BEAM = 0) veto was introduced. The efficiency turned out to be 0.94 ± 0.01.

C. Muon Veto Efficiency

Muon veto efficiency was also estimated using the $Z + 2j$ sample similar in topology and random muon track rate. The calculations were done using the event count in the Z peak before and after th muon veto was applied. Background under the Z was subtracted using the sideband method. Muon veto efficiency is 0.97 ± 0.01.

D. Electron ID Efficiencies

The electron identification efficiency as well as the efficiencies of event quality cuts were determined using the $Z+2j$ events which are very similar in topology and chamber occupancy to the signal sample. Details of the calculations can be found in [2]. It is important to use the events with similar jet multiplicity since the $eejj$ analysis showed that the electron ID efficiency deteriorates in high occupancy environments. The combined efficiency of the revertexing and electron ID requirement was shown to be 0.61 ± 0.04% in CC and 0.54 ± 0.04% in EC in agreement with the individual efficiencies obtained in the $eejj$ analysis [2]. Average electron ID efficiency for the LQ signal was obtained by accounting for the fact that the fraction of LQ signal events which pass basic cuts described above and have the electron in CC is virtually independent of the LQ mass and equals to 0.93 ± 0.01. The individual and combined tracking and ID cut efficiencies are summarized in Table IV.

VII. BACKGROUNDS

A. Top Background

Top background was determined from the MC sample described in Section V C. All the basic cuts except for the muon veto and active main ring veto were applied to this sample. The muon veto efficiency for top is much lower than that for the LQ sample since it is expected that top events will give real muons in the final state due to $W \to \mu\nu$ decays and cascade b-quark decays.

The efficiency of muon veto for top events was studied in great detail by the top group [12]. It was shown that the GEANT overestimates the rejection factor against the muons, and the corrections depending on the run number and muon rapidity are between 0.5 and 0.9 (see Ref. [12] for details). These corrections were then applied to the efficiency of the muon veto cut as measured from the top MC. Averaged in rapidity and integrated luminosties of the different run ranges the overall muon rejection factor was found to be 1.9 ± 0.1. This value was obtained by correcting the rejection of the muon veto as measured by applying veto requirements to the $t\bar{t}$ MC sample with additional factor [12] reflecting differences in the CF and EF muon chamber efficiency in GEANT and in pre/post-shutdown data.

This factor together with efficiencies, and CCEM crack corrections (see Ref [2] for details) were then applied to the MC data to give the overall top background in the base sample of 2.0 ± 0.7 events where the 35% systematic error is dominantly due to the error on the top cross section as measured by DØ [19] and jet energy scale.

B. QCD background

QCD background was determined using the QCD mini-stream discussed in Section V D.

We first determined the jet faking electron probability in the very same way it was done in the $eejj$ analysis [2]. The jet faking an electron probability was calculated by comparing the number of electrons with $E_T^{\mathrm{EM}} > E_0$ which pass standard quality cuts with the total number of jets with $E_T^j > E_0$ in the QCD stream. The E_0 threshold was varied from 20 to 50 GeV and the probabilities were shown to be stable with the cut value above 25 GeV, i.e. above the jet trigger turn-on. The jet faking electron probability was measured to be:

$$f_e = (3.50 \pm 0.35) \cdot 10^{-4}$$

and is independent of E_T^{EM} and the rapidity of the EM object within the errors. It was also cross-checked by taking the ratio of $3j$+EM and $4j$ events. The method used for faking probability estimate automatically accounts for direct photon background which is a part of general multijet background. Since the ID cuts on the electron are rather tight we have not required this electron to pass signal trigger L2 requirements. We have checked that the trigger inefficiency is small, so that if we overestimate fake probability because of this effect, we do it by $< 10\%$, i.e., within the assigned errors.

We further selected a subsample of ≥ 3 jet events in the QCD stream by requiring the event to have at least three jets and $\not\!\!E_T > 30$ GeV. Since we use electron-based revertexing in the data which ensures us that the correct vertex is picked, we have to ensure the same for the QCD background sample. The easiest way to do so is to restrict ourselves to a sample of events with a single interaction which occured in a good fiducial volume of the central tracker. In order to do so we required the events to have a single reconstructed vertex within a good fiducial volume of the detector (-50 cm $< Z_{\rm vtx} <$ 50 cm). Since Run IB events have high probability of multiple interactions and multiple reconstructed vertices, and additional correction factor due to this cut was determined with $Z + 2j$ data to be 2.2 ± 0.2. This number was obtained by counting the fraction of single-interaction events in the $Z+2j$ data as a function of luminosity and weighting it with a luinosity profile of the QCD data stream. It also agrees well with the number obtained from the QCD stream itself (before signal cuts which bias the choice of vertex are applied).

Difference in the average instantaneous luminosity of the QCD and $Z + 2j$ samples is taken into account. The result also agrees with the scaling factor calculated just from the QCD data.

The distribution in the azimuthal angle of the $\not\!\!E_T$ vector for this subsample is shown in Fig. 2a. An apparent (and unexpected) feature in this plot (apart for small bumps at $\phi \approx 1.8$ and 5.0 — in the direction of the Main Ring and opposite to it) is a huge peak at $\phi \approx 2.5$. Further investigation uncovered that the events in the peak originate from 20 bad runs where apparently there was a hot cell in the calorimeter in the direction opposite to the peak position. These runs were not marked as bad in the standard DØ bad run list. We, however, cross-checked all of them against the control room logbooks and found that for majority of these runs calorimeter problems and suggestion of a bad BLC board was logged. Finally, the bad BLS card was replaced right after the last of the bad runs and that ended the hot cell problem in Run IB. This information therefore might be of interest for anyone who is doing analysis which requires significant $\not\!\!E_T$. We have listed the run numbers and their integrated luminosities for signal and background triggers in Table V. Total luminosity of the additional bad runs for the signal trigger is only 0.8 pb^{-1}. After removal of these bad runs the distribution in the azimuthal angle of the $\not\!\!E_T$ vector in the QCD sample looks reasonable (see Fig. 2b).

We then looped over all possible three-jet combinations, treating one of the jets as if it was an electron, and required that the combination pass our kinematic and fiduical cuts for the "electron" and jets. The combinations were not required to pass the electron ID cuts, since these cuts are already accounted for in the QCD faking probability. QCD background was then estimated by multiplying number of combinations by the jet faking electron probability and a normalization factor which accounts for differences in the QCD sample and data sample luminosities.

Number of three-jet combinations passing certain requirements is summarized in Table VI. Total QCD background in the base sample turned out to be 4.1 ± 1.0 events. The background error accounts for both statistics in the QCD sample and 20% systematic error which reflects the variation of faking probabilities with E_T^e and between CC and EC, as well as the jet trigger turn-on effects and uncertainty on the scaling factor.

C. $W+2j$ Background

The dominant $W+2j$ background was calculated using the MC. It is extremely important therefore to make sure that the MC models data properly, or otherwise the rejection of the high cut on the $M_T^{e\nu}$ as well as the network behavior against this background won't be modeled properly.

A comparison of the various kinematical distributions for the data and the $W+2j$ MC showed that the MC distributions, being similar in shape are offset relative to the data ones. In order to eliminate such an offset we tuned both hadronic and electromagnetic energy scales in the MC events until a proper agreement was achieved. The scale for the EM calorimeter was determined by comparing the $Z+2j$ data with the MC (see [2] for details on the Drell-Yan MC samples). Position of the peak in the data stays the same within the errors for different topological combinations: CC-CC, CC-EC, and EC-EC which is illustrated in Fig. 3 and simply reflects the proper EM energy scale tuning using much higher inclusive Z statistics. The position of the peak in the MC samples is systematically shifted down and shows statistically significant topological dependence (see Fig. 4). By comparing the average position of the Z-peak in the data and in three topological MC samples we conclude that the CCEM calorimeter should be scaled up by 3%, and the ECEM should be scaled up by 1%. Such a boos of the MC EM energy scale correctly offsets the observed -3%, -2% and -1% shift in the Z-peak position for CC-CC, CC-EC, and EC-EC combinations respectively. After fixing the EM energy scale we obtained a reasonable agreement between the data and the sum of QCD/top backgrounds and $W+2j$ MC with nominal jet energy scale. Figure 5 illustartes the agreement between the data and the sum of the backgrounds for all basic cuts except for the $M_T^{e\nu}$-cut applied to both. The vertical scale of the $W+2j$ MC distributions was tuned to match the data. The scaling factor applied to the raw MC events turned out to be 0.22 ± 0.01, which is close to the one expected from pure cross section and efficiency calculations (0.20). Apart from slight differences close to the cut thresholds (due to turn-on and resolution effects) the agreement between the data and the background prediction is good. Similar conclusion was reached by performing a Bayesian fit of several kinematical distributions to a sum of QCD and $W+2j$ background.

To check our understanding of the relative fractions of the QCD and $W+2j$ backgrounds we repeated the comparison with looser (25 GeV) and tighter (35 GeV) cuts on the $\not{E}_T$ in all samples. The energy scale and normalization used were exactly the same as determined for the main sample. The results are shown in Figs. 6, 7 and prove that fractional backgrounds are known well enough (the QCD background fraction varies by a factor of 6 for $\not{E}_T$ cuts between 25 and 35 GeV: from 115 to 20 events).

The two most important distributions for which the cuts were applied: the $M_T^{e\nu}$ and S_T^{12} are shown on the log scale in Fig. 8. It is clear that we model the transverse mass distribution quite well up to the values of the cut; the S_T^{12} distribution is also well understood except for the lower tail where MC has a systematically offset turn-on.

The described method of scaling the background to the data gives low systematics errors due to the energy scale, since the latter has been already adjusted to match the data. The background uncertainty is due dominantly to the uncertainty on the scaling factor and equals 7%.

We determined the number of the $W+2j$ background events in the base sample to be

11.7 ± 1.8.

D. Total background

The total background estimate after basic cuts is 18 ± 2 events, which is in agreement with 14 events observed in the data.

VIII. NEURAL NETWORK ANALYSIS

Random grid search analysis was performed with many combinations of variables. Since S_T^{12} and $dM/M(180)$ were shown to be the most powerful variables for separating high mass LQ signal from top, $W+2j$ and QCD backgrounds, we used these variables as inputs in the neural network analysis. We used a three layer feed-forward neural network (NN) with 2 input nodes—corresponding to the variables S_T^{12} $(= E_T^e + E_T^{j1} + E_T^{j2} + \not{E}_T)$ and $dM/M(180)$, 5 hidden nodes and 1 output node. The network was trained using the 160 GeV and 180 GeV leptoquark MC samples as the signal (with a desired network output $\mathcal{D}_{NN} = 1$) and the expected admixture of W+jets, QCD fake and $t\bar{t}$ events as the background (with $\mathcal{D}_{NN} = 0$). As is clear from Fig. 9, a significant discrimination between signal and background was achieved. We further showed that the neural network using the two variables performed better than applying cuts independently on them.

A crucial point in the NN approach is our understanding of the $\mathcal{D}_{NN}$ distribution of the backgrounds. We have already shown that the one of the two components, S_T^{12}, is described reasonably well by the backgrounds in the loose data sample. We further studied the $\mathcal{D}_{NN}$ distribution in this sample explicitly and compared it with the expected sum of three major backgrounds. An excellent agreement between the two is illustrated in Fig. 10.

Each value of the NN output, which approximates the ratio $\frac{s(x)}{s(x)+b(x)}$ ($s(x)$ and $b(x)$ being the 2-dimensional signal and background densities), defines an equiprobability contour between the signal and background in the $(S_T^{12}, dM/M(180))$ space. This contour represents the desired optimal function linking S_T^{12} and $dM/M(180)$. The expected distribution in $x \equiv (S_T^{12}, dM/M(180))$ for leptoquark signal at various masses with loose cuts applied are shown in Fig. 11. The distributions for the three types of background samples with loose cuts applied are shown in Fig. 12. These figures also show the NN equiprobability contours corresponding to the values $\mathcal{D}_{NN}$ =0.6, 0.7, 0.8, and 0.9.

After applying the basic cuts the distributions for the signal do not change much, but the background is different. The three components of the backgrounds and the NN equiprobability contours for the base cuts are shown in Fig. 13. Finally, Fig. 14 shows the comparison between the data, LQ signal with mass of 200 GeV and the expected sum of all the backgrounds. Data clearly prefers background interpretation. The equiprobability contours correspond to the values $\mathcal{D}_{NN} = 0.75$, 0.85, and 0.95 in these figures.

It is clear from the plots for background that due primarily to the top background which populates high S_T^{12}, a mass window cut is essential to keep the overall background under control. This was different in the $eejj$ analysis where S_T turned out to be a sufficient variable. We conclude that the use of the mass-difference variable is essential for the present analysis due to the entirely different background components in the $e\nu jj$ channel.

Since we see no evidence for the LQ signal, we proceed with the limit setting strategy by optimizing the signal given fixed background of ≈ 0.4 events which, given the absence of the LQ signal, with 67% probability results in no events in the data. Such a value of the background is achieved for the cut on the NN discriminant $\mathcal{D}_{NN} > 0.85$, which corresponds to 0.29 ± 0.25 events expected from the background. No events in data satisfy this cut.

A good agreement between the data and expected background as a function of the $\mathcal{D}_{NN}$ is shown in Fig. 9. Actual values of each background with their errors as well as total background are listed in Table VII.

A few other neural networks as well as a rectangular cuts on the S_T^{12} and $dM/M(180)$ were also tried in the course of this analysis. All the networks that gave a background of about 0.4 events resulted in either zero or one events in the data, consistent with the expectations. Their efficiencies were, however, significantly or somewhat less than that for the final network used in this analysis. For rectangular cuts a background of 0.4 events is achieved for the $S_T^{12} > 350$ GeV and $dM/M(180) < 0.25$. This set of cuts also results in no events in the data but has about 10% less efficiency at $M_{LQ} = 180 GeV$.

Neural net output and other parameters of all fourteen events in the base sample are given in Table VIII.

IX. SIGNAL SYSTEMATICS

The systematic errors used in the subsequent sections for derivation of the limits on signal were obtained by comparing acceptance for the signal in several signal samples generated with ISAJET and PYTHIA with different structure functions and Q^2 scale. An uncertainty due to jet energy scale was derived by varying the jet response by $\pm 1\sigma$ (i.e., $E_{high} = 1.04 * E + 1.0$ GeV and $E_{low} = 0.96 * E - 1.0$ GeV). The systematic errors on the signal varies from 25% to 8% for the LQ masses between 80 and 220 GeV. Systematic uncertainties are summarized in Table IX. (This table summarizes uncertainties for the envelope limits, see Section XI; for $dM/M(180)$-only network the errors vary between 8% and 40% with the minimum around $M_{\rm LQ} = 180$ GeV).

The fact that the neural network used S_T^{12} defined by the two leading jets and not the all-jets-based S_T significantly decreases signal systematics due to jet energy scale and initial/final state radiation.

X. SIGNAL ACCEPTANCE

Signal acceptance was calculated from MC using a mixture of the ISAJET and GEANT information to account for the effect of the CCEM cryostat ϕ-cracks improperly treated by GEANT (see Ref. [2] for detailed discussion). Mixture method gives acceptance numbers about 5% higher than based on the GEANT-only information, in agreement with what was found in the course of $eejj$ analysis and by other studies.

Acceptance numbers before and after the $\mathcal{D}_{NN} > 0.85$ cut as well as the overall detection efficiency are summarized in Table X. The last two columns include the systematic errors described above.

XI. RESULTS

Since we do not find a significant excess of events above the background for various cuts on the NN output $\mathcal{D}_{NN}$ of the $dM/M(180)$ network, we choose the cut ($\mathcal{D}_{NN} > 0.85$) which yields ≈ 0.4 background events, à la limit setting strategy discussed in detail in Ref. [2]. With this cut no data events survive (the last event is at $\mathcal{D}_{NN} = 0.79$), while we would expect 2.7 leptoquark events if the leptoquark mass was 180 GeV. From the acceptances and efficiencies in Table X, an integrated luminosity of 115 ± 6 pb^{-1}, we have computed the 95% upper limits on the cross section. The upper limits are given in Table XI. When we compare these limits with the lower bound of the theoretical cross section [16] we obtain a lower limit of 175 GeV, at 95% CL, on the leptoquark mass, assuming $\beta = 1/2$ (see Fig. 15).

In order to increase sensitivity for the lower and higher LQ masses where the limits on the $\beta < 1/2$ or combined $eejj + e\nu jj$ limits are achieved, we have repeated the neural network training described above for different central masses of the dM/M mass window. The $dM/M(80)$, $dM/M(100)$, $dM/M(120)$, $dM/M(140)$, $dM/M(160)$, $dM/M(200)$, and $dM/M(220)$ networks were formally trained and the backgrounds as function of the NN discriminant were calculated. For these additional networks a significant separation between the signal and the backgrounds was also achieved. We expect the network based on a particular LQ mass scale to be the most efficient among other networks around this mass. It is in fact true for the LQ masses above approximately 140 GeV.

All four additional neural networks with $M_{LQ} \geq 140$ with the $\mathcal{D}_{\rm NN} > 0.80$ cut correspond to the predicted backgrounds between 0.41 ± 0.27 and 0.61 ± 0.27 events and zero observed events in the data. (Same is true for the lower masses network as well.) In setting the cuts we used a step of 0.05 in $\mathcal{D}_{\rm NN}$ and used the value most consistent with the desired background level of 0.4 within the errors on the background. Table XII shows the backgrounds for cuts on $\mathcal{D}_{\rm NN} > 0.80$ and 0.85 and illustrates the method used for choosing the cut.

The predicted background agrees with the observed data as a function of the discriminant well (similar to the $dM/M(180)$ network discussed in detail above). As expected the additional networks gain sensitivity of this search at the lower masses, close to the center value of the used window. The networks limits are quite smooth function of the mass window, which allows us to use an envelope which surrounds all the single-NN-based limits as the final result of this search.

For the networks based on the $M_{\rm LQ} < 120$ GeV masses it turned out that the separation between the signal and background is achieved only at the very tail of the signal, so the efficiency of such a network for signal is very sensitive to uncertainties on jet energy scale and signal modelling. Because of this systematic error on efficiency reaches 50% at low masses. We therefore decided to use a more stable approach based on our experience gained in the course of the $eejj$ analysis. We notice that the only reason of using dM/M variable in the networks is to suppress the top background. However, for low LQ masses this background is not important, since dominant components are QCD and $W + 2j$ production, which is ismilar to $eejj$ case. We know that the S_T^{12} variable by itself is very efficienct against these backgrounds. Therefore for low masses we used a simple S_T^{12} cut to set the limits, analogous to the $eejj$ analysis. As we showed before, the S_T^{12} distribution of the data events is described quite well with the background predictions, especially at high S_T^{12}. A cut $S_T^{12} > 400$ GeV corresponds to a background prediction of 0.60 ± 0.27 events, consistent with the desired level of 0.4 events. It leaves zero events in the data with the highest S_T^{12} event being at $S_T^{12} = 388$ GeV, consistent with the background expectations.

NN contours for input LQ masses between 120 and 200 GeV together with the $S_T > 400$ GeV results and the envelope limit from this analysis are shown in Fig. 16. Numerical values of the efficiencies and the cross section limits for these networks and S_T-cut are listed in Table XIII. The figure and the table also illustrate the deterioration of the limits based on the low mass (120 GeV) network due to increased systematic error on the efficiency. The final limit from this experiment is therefore given by the envelope contour shown in Fig. 16 with the dashed line and separately in Fig. 17. The values of the envelope limit as a function of the LQ mass are given in Table XIV.

Combined mass versus β limit plots with all three channels ($eejj$, $e\nu jj$ and $\nu\nu jj$ [20]) add together was obtained by combining likelihoods of all three measurements with common systematics taken into account. The limit combination program, used in [13] was used.

Efficiencies, backgrounds, and individual cross section limits for all three channels used in combination are summarized in Tables XIV,XV,XVI. The 95% CL lower mass limit on first generation scalar leptoquark from this combined data set is shown as a function of β in Fig. 18. It excludes existence of the LQ with masses below 200 GeV for $\beta 0.4$. For $\beta = 1/2$ allowed by canonic LQ models the lower mass limit is 204 GeV (see Fig. 20).

Extension of the optimized $eejj$ and $e\nu jj$ analyses to even lower masses, between LEP limit [21] of 45 GeV and this analysis lower mass point of 80 GeV, is quite meaningless, since both the background and signal cross sections are very high in this region (e.g., signal cross section for $M_{\mathrm{LQ}} = 60$ GeV is 0.16 nb, so even for low values of β one would expect light LQ to be produced copiously). Therefore, the optimization criteria of obtaining low ($\approx$ 0.4 events) background and maximizing the signal efficiency does worse job than a simple significance ($S/\sqrt{B}$) optimization and also requires much larger MC signal sample for accurate measurement of a very low signal efficiency.

Nevertheless, it is very important to close the "gap" between the region excluded by LEP and 80 GeV (apart from the $\nu\nu jj$ exclusion contour for $\beta < 0.35$). In order to do so we first of all note that our previous published limit from Run IA $eejj + e\nu jj$ channels [22] (shown in Fig. 18 with a this solid line) closes the "gap" for any $\beta > 0.15$. We can further use an "unoptimized" analysis based on the 14 event sample used in the $e\nu jj$ analysis in order to close the "gap" for even lower values of β. Indeed, in a (crazy) assumption that all 14 events are due to the LQ signal, the upper 95% CL limit on the cross section times branching ratio times efficiency is 0.20 pb (this number takes into account 10% systematic error due to the luminosity, jet energy scale, particle ID, and MC modelling uncertainties). Using the overall efficiencies before the $\mathcal{D}_{\mathrm{NN}}$ cut, summarized in Table XVII, one can exclude certain range of β values as a function of the LQ mass, as shown in the table and in Fig. 18. Being quite conservative this "unoptimized" exclusion contour nevertheless basically closes the gap between LEP and the combined optimized analysis for all values of β.

A "cleaned-up" version of the mass vs. beta exclusion plot is obtained by eliminating areas below our previously excluded limits [22] and extending the $e\nu jj$ results 5 GeV below the lowest MC point via scaling down the cuts values. It is shown in Fig. 19 and represents the main result of this work.

The results of this combined analysis make an explanation of HERA data with scalar first generation leptoquark extremely unlikely [23].

[1] S. Abachi *et al.*(DØ Collaboration), preprint Fermilab–Pub–97/252–E, to appear in Phys. Rev. Lett. **B**.
[2] P. Bhat *et al.*, DØ Note #3208 (unpublished).
[3] K.S. Babu *et al.*, hep-ph/9705414 (unpunblished).
[4] J.L. Hewett, private communication.
[5] C. Adloff *et al.*(H1 Collaboration), preprint DESY 97–024 (1997), submitted to Z.Phys. **C**. J. Breitweg *et al.*(ZEUS Collaboration), preprint DESY 97–025 (1997), submitted to Z.Phys. **C**.
[6] J. Hewett, T.G. Rizzo, "Much Ado About Leptoquarks," preprint SLAC–Pub–7430, submitted to Phys. Rev. **D**.
[7] J. Whitman, for the DØ Collaboration, presented at LaThuile 1997; J. Hobbs, for the DØ Collaboration, presented at New Physics: Moriond 1997.
[8] D. Norman, for the DØ Collaboration, presented at HCP'97, Stony Brook, June 1997.
[9] I. Adam, D0 Note # xxxx, unpublished.
[10] CAFIX 5.0 reference.
[11] U. Heintz, D0 Note # xxxx, unpublished.
[12] J. Cochran, "$e\mu$ truth in Run I," http://www-d0.fnal.gov/˜cochran/d0_private/top_emu.html
[13] G. Wang, DØ Note 3185, unpublished; J. Hobbs, G. Wang, DØ Note ???? (unpublished).
[14] R. Brun and F. Carminati, CERN Program Library Writeup W5013, 1993 (unpublished); we used GEANT v3.15.
[15] T. Sjöstrand, Comp. Phys.Comm. **82**, 74 (1994).
[16] M. Krämer *et al.*, Phys. Rev. Lett., **79**, 341 (1997).
[17] F.A. Berends *et al.,* Nucl. Phys. B **357**, 32 (1991).
[18] G. Marchesini *et al.*, Comp. Phys. Comm. **67**, 465 (1992); we used HERWIG v5.7.
[19] S. Abachi *et al.*(DØ Collaboration), to be published in Phys. Rev. Lett., Fermilab-Pub-97/109-E, `hep-ex/9704015`; *ibid.*, to be published in Phys. Rev. Lett., Fermilab-Pub-97/059-E, `hep-ex/9703008`.
[20] S. Abachi *et al.*(DØ Collaboration), Phys. Rev. Lett. **76**, 2222 (1996); D. Claes and E. Flattum `http://www-d0.fnal.gov/www_buffer/new_phenomena/stop/lq_doc_v131.ps`.
[21] see, e.g. P. Mättig, preprint CERN–PPE/96-187.
[22] S. Abachi *et al.*(DØ Collaboration), Phys. Rev. Lett. **72**, 965 (1994).
[23] J.L. Hewett, T.G. Rizzo, preprint SLAC-Pub-7549; `hep-ph/9708419`.

Run	Trigger Name	Trigger Requirements	$\int L dt$	N Events
Run 1A	ELE_HI	$E_T^{EM} > 20$ GeV	11.2 pb^{-1}	9,862
Run 1B	EM1_EISTRKCC_MS	$E_T^{EM} > 20$ GeV, ISO $\not{E}_T > 15$ GeV	92.9 pb^{-1}	77,912
Run 1C	EM1_EISTRKCC_MS	$E_T^{EM} > 20$ GeV, ISO $\not{E}_T > 15$ GeV	0.8 pb^{-1}	369
Run 1C	ELE_JET_HIGHA	$E_T^{EM} > 17$ GeV, ISO $E_T^{J1,2} > 10$ GeV,$\not{E}_T > 14$ GeV	10.5 pb^{-1}	7,240

TABLE I. The Level 2 triggers used in the first generation LQ $e\nu jj$ analysis, their definitions, integrated luminosities and the starting number of events in the extended data set.

Cut	Number of events
Preselection	95,383
No bad runs	90,998
Cal_Recovery & Good_Beam	68,890
Revertexing info	34,086
Only one electron	22,649
$E_T^e > 20$ GeV	21,176
Electron in CC or EC	18,683
$N_j(\lvert\eta_d^j\rvert < 2.5, E_T^j > 20 \text{ GeV}) \geq 2$	8,925
Electron ID	3,091
Muon Veto	2,963
$\not{E}_T > 30$ GeV	1521
$\not{E}_T$ isolation cut	1314
$M_T^{e\nu} > 110$ GeV	14

TABLE II. Event selection.

MLQ in GeV	No. MC evts	Cross sec.
80	5000	19.60 pb
100	3000	12.60 pb
120	3000	4.454 pb
140	3000	1.803 pb
160	4999	0.793 pb
180	4996	0.373 pb
200	1999 1998 (PYTHIA)	0.184 pb
220	4996	0.093 pb

TABLE III. LQ Monte Carlo event samples.

Requirement	CC	EC	Average
Matching track	0.70 ± 0.03	0.80 ± 0.05	0.71 ± 0.03
$\varepsilon_5 < 1.0$	0.87 ± 0.02	0.68 ± 0.03	0.86 ± 0.02
Total ID	0.61 ± 0.03	0.54 ± 0.04	0.60 ± 0.03

TABLE IV. Electron ID efficiencies and individual tracking and quality cut efficiencies from the $Z + 2j$-sample.

Run No.	$\int Ldt$ for EM1_EISTRKCC_MS	$\int Ldt$ for JET_3_MON
75878	2.3097E-01 nb^{-1}	2.2940E+00 nb^{-1}
76721	3.3454E-01 nb^{-1}	8.1940E+00 nb^{-1}
76815	1.2127E+00 nb^{-1}	6.0635E+00 nb^{-1}
76816	7.8326E-01 nb^{-1}	3.9163E+00 nb^{-1}
76817	7.5409E-01 nb^{-1}	3.7705E+00 nb^{-1}
85330	1.1919E+00 nb^{-1}	6.7533E+01 nb^{-1}
85406	9.9596E-01 nb^{-1}	5.7558E+01 nb^{-1}
85411	8.9513E-02 nb^{-1}	5.0220E+00 nb^{-1}
85798	1.6378E+00 nb^{-1}	4.7774E+01 nb^{-1}
85837	7.8337E-01 nb^{-1}	4.5888E+01 nb^{-1}
85963	1.2027E+00 nb^{-1}	6.9415E+01 nb^{-1}
86518	1.2267E+00 nb^{-1}	7.2926E+01 nb^{-1}
86532	3.4331E-02 nb^{-1}	5.1607E+00 nb^{-1}
86535	1.0199E+00 nb^{-1}	5.9094E+01 nb^{-1}
86537	1.4839E+00 nb^{-1}	4.3012E+01 nb^{-1}
86549	5.5710E-01 nb^{-1}	8.3598E+01 nb^{-1}
86551	2.0718E+00 nb^{-1}	5.9044E+01 nb^{-1}
86862	5.7985E-01 nb^{-1}	8.1686E+01 nb^{-1}
86864	8.1302E-01 nb^{-1}	4.5828E+01 nb^{-1}
86919	8.0959E-01 nb^{-1}	4.0926E+01 nb^{-1}
Total $\int Ldt$	0.81 pb^{-1}	0.018 pb^{-1}

TABLE V. Parameters of the additional Run IB bad runs

Cut	Number of events/jet combinations
Starting sample	356,415
Three jet requirement	324,601
Bad run veto	323,288
$\not{E}_T > 20$ GeV	11,778
Total combinations	41,377
Electron kinematic/fiducial cuts	14,534
Jet kinematic/fiducial cuts	13,567
$\not{E}_T > 30 GeV$	481
$M_T^{e\nu} > 110$ GeV	43

TABLE VI. Number of events/jet combinations in the QCD background sample.

NN cut	N $W+2j$	N Top	N QCD	Bck. W+2j	Error	Bck. Top	Error	Bck. QCD	Error	Total bck.	Error	Data
0.00	53	1773	43	11.7	1.8	1.97	0.69	4.13	1.04	17.8	2.2	14
0.05	42	1719	42	9.24	1.57	1.91	0.67	4.04	1.02	15.2	2.0	13
0.10	33	1473	38	7.26	1.36	1.64	0.57	3.65	0.94	12.6	1.8	10
0.15	30	1300	36	6.60	1.29	1.44	0.51	3.46	0.90	11.5	1.7	9
0.20	27	1187	33	5.94	1.22	1.32	0.46	3.17	0.84	10.4	1.6	7
0.25	24	1092	30	5.28	1.14	1.21	0.42	2.88	0.78	9.38	1.45	7
0.30	20	1007	26	4.40	1.03	1.12	0.39	2.50	0.70	8.02	1.31	6
0.35	19	929	22	4.18	1.00	1.03	0.36	2.12	0.62	7.33	1.23	4
0.40	17	855	19	3.74	0.94	0.95	0.33	1.83	0.56	6.52	1.14	4
0.45	12	797	18	2.64	0.78	0.89	0.31	1.73	0.53	5.26	1.00	4
0.50	11	738	17	2.42	0.75	0.82	0.29	1.63	0.51	4.87	0.95	3
0.55	11	652	13	2.42	0.75	0.72	0.25	1.25	0.43	4.39	0.90	3
0.60	8	579	12	1.76	0.63	0.64	0.23	1.15	0.41	3.56	0.79	3
0.65	7	515	8	1.54	0.59	0.57	0.20	0.77	0.31	2.88	0.70	3
0.70	6	438	6	1.32	0.55	0.49	0.17	0.58	0.26	2.38	0.63	3
0.75	5	356	5	1.10	0.50	0.40	0.14	0.48	0.24	1.98	0.57	1
0.80	2	269	1	0.44	0.31	0.30	0.10	0.10	0.10	0.83	0.34	0
0.85	0	176	1	0.00	0.22	0.20	0.07	0.10	0.10	0.29	0.25	0
0.90	0	89	1	0.00	0.22	0.10	0.03	0.10	0.10	0.19	0.24	0
0.95	0	26	1	0.00	0.22	0.03	0.01	0.10	0.10	0.13	0.24	0

TABLE VII. Data and predicted background as a function of the $\mathcal{D}_{NN}$ cut.

Run/Event	E_T^e	$\not\!\!E_T$	E_T^{j1}	E_T^{j2}	S_T^{12}	$dM/M(180)$	$M_{\rm fit}$	$\mathcal{D}_{NN}$
82298/ 9717	65.8	48.5	47.4	40.4	202.0	0.21	148.3	0.32
82341/ 4310	40.2	145.5	90.6	48.1	324.5	0.52	91.7	0.26
83236/11344	86.5	41.4	41.1	38.5	207.5	0.36	115.0	0.08
87063/26923	105.8	33.4	97.3	24.5	260.9	0.65	54.0	0.13
88321/15193	76.9	64.4	34.2	25.6	201.1	0.34	115.9	0.09
88470/ 4236	127.3	31.8	75.4	53.1	287.6	0.11	216.2	0.75
89708/24871	61.9	93.2	62.0	54.5	271.6	0.36	120.2	0.18
90401/ 1772	120.1	44.2	79.3	41.1	284.6	0.07	185.6	0.74
90455/ 1247	46.2	66.5	108.4	95.3	208.1	0.50	206.6	0.06
90698/ 7682	58.9	64.2	24.9	29.5	177.5	0.64	66.1	0.05
91933/ 1552	126.5	83.7	47.5	43.1	300.9	0.07	131.1	0.79
92276/ 5931	74.3	50.6	109.2	111.0	235.9	0.30	241.8	0.19
94598/ 5342	67.9	157.3	119.8	42.5	387.6	0.46	107.3	0.46
95491/10720	62.2	124.7	65.3	68.7	255.7	0.34	207.3	0.34

TABLE VIII. Parameters of 14 events in the base sample

Source of systematics	Uncertainty
Particle ID	5%
Smearing in the Detector	3%
Jet energy scale	2%-10% (for $M_{\rm LQ}$ = 80–220 GeV)
Gluon radiation	4%
PDF and Q^2 scale	5%
MC statistics	3-25% (for $M_{\rm LQ}$ = 80–220 GeV)
Luminosity	5%
Total	8%-25% (for $M_{\rm LQ}$ = 80–220 GeV)

TABLE IX. Signal systematics.

LQ Mass, GeV	Acceptance, base cuts	Acceptance, $\mathcal{D}_{\mathrm{NN}} > 0.85$	Overall Efficiency
80	6.1%	$0.6 \pm 0.2\%$	$0.3 \pm 0.1\%$
100	12.9%	$1.8 \pm 0.4\%$	$1.0 \pm 0.2\%$
120	19.7%	$3.6 \pm 0.6\%$	$2.0 \pm 0.3\%$
140	26.5%	$7.1 \pm 1.7\%$	$3.9 \pm 1.0\%$
160	32.7%	$18.5 \pm 2.8\%$	$10.1 \pm 1.6\%$
180	36.7%	$26.8 \pm 2.1\%$	$14.7 \pm 1.2\%$
200	42.1%	$34.0 \pm 3.1\%$	$18.6 \pm 1.8\%$
220	44.9%	$34.5 \pm 6.9\%$	$18.9 \pm 3.8\%$

TABLE X. Signal kinematical and geometrical acceptance and the overall detection efficiency as a function of the LQ mass for the $dM/M(180)$ network.

Mass (GeV)	95% C.L. c.s upper limit (pb)	Low NLO c.s. pb
80	69.5	17.98
100	3.43	5.34
120	1.48	1.90
140	0.88	0.77
160	0.29	0.34
180	0.18	0.16
200	0.15	0.08
220	0.17	0.04

TABLE XI. Upper limits on the leptoquark production cross section and comparison with the NLO cross section [16] for $\beta = 1/2$ as a function of the leptoquark mass for the $e\nu jj$ channel. Limits are based on the $dM/M(180)$ network only.

dM/M Mass Scale (GeV)	Background for $\mathcal{D}_{\mathrm{NN}} > 0.80$ cut	Background for $\mathcal{D}_{\mathrm{NN}} > 0.85$ cut
140	0.51 ± 0.25	0.22 ± 0.24
160	0.61 ± 0.27	0.21 ± 0.24
180	0.83 ± 0.34	0.29 ± 0.25
200	0.43 ± 0.27	0.26 ± 0.25
220	0.41 ± 0.27	0.24 ± 0.25

TABLE XII. Background for two different $\mathcal{D}_{\mathrm{NN}}$ cuts as a function of dM/M scale used in the networks. Bold numbers correspond to the cut chosen for a particular network.

LQ Mass	$S_T^{12} > 400$ GeV		$dM/M(120)$		$dM/M(140)$		$dM/M(160)$		$dM/M(180)$		$dM/M(200)$		$dM/M(220)$	
GeV	ϵ	σ^{95}, pb	ϵ	σ^{95}, pb	ϵ	σ^{95}, pb	ϵ	σ^{95}, pb	ϵ	σ^{95}, pb	ϵ	σ^{95}, pb	ϵ	σ^{95}, pb
80	***0.32%***	***10.875***	0.03%	2177	0.21%	238.3	0.18%	295.2	0.33%	69.49	0.45%	17.59	0.42%	31.63
100	***1.15%***	***2.586***	0.38%	61.33	0.68%	9.712	0.97%	3.38	0.97%	3.434	1.17%	2.572	1.07%	2.858
120	***2.45%***	***1.148***	1.98%	1.637	2.24%	9.01	1.68%	1.777	1.96%	1.476	2.49%	1.137	2.38%	1.214
140	4.42%	0.623	4.50%	0.793	***6.65%***	***0.427***	5.52%	0.84	3.89%	0.876	4.30%	0.658	4.00%	0.707
160	7.61%	0.355	3.53%	1.116	8.88%	0.338	***10.93%***	***0.253***	10.15%	0.286	9.43%	0.302	8.05%	0.351
180	11.03%	0.292	3.49%	0.794	7.77%	0.531	14.07%	0.192	***14.67%***	***0.183***	14.60%	0.185	12.88%	0.215
200	14.51%	0.186	4.24%	0.661	6.28%	0.456	13.21%	0.251	18.63%	0.146	***19.37%***	***0.139***	18.48%	0.147
220	19.09%	0.141	4.74%	0.576	6.18%	0.439	9.09%	0.305	18.94%	0.165	21.97%	0.122	***21.54%***	***0.125***

TABLE XIII. Efficiency and corresponding 95% CL limits on the leptoquark production cross section for different networks and $S_T^{12} > 400$ GeV cut used in the analysis. Highlighted numbers are the one used for making the envelope limits.

Mass (GeV)	Efficiency (%)	Background (Events)	95% C.L. c.s upper limit (pb)	Low NLO c.s. times branching ratio (pb)
80	0.32 ± 0.08	0.60 ± 0.27	10.9	18.0
100	1.15 ± 0.21	0.60 ± 0.27	2.6	5.34
120	2.45 ± 0.33	0.60 ± 0.27	1.0	1.90
140	6.65 ± 0.96	0.54 ± 0.25	0.43	0.77
160	10.9 ± 1.2	0.61 ± 0.27	0.24	0.34
180	14.7 ± 1.2	0.29 ± 0.25	0.18	0.16
200	19.4 ± 1.7	0.43 ± 0.27	0.14	0.08
220	21.5 ± 1.7	0.41 ± 0.27	0.12	0.04

TABLE XIV. Efficiency, background, upper limit on the leptoquark production cross section, and comparison with the NLO cross section [16] times branching ratio for $\beta = 1/2$ as a function of the leptoquark mass for the $e\nu jj$ channel.

Mass (GeV)	Efficiency (%)	Background (Events)	95% C.L. c.s upper limit (pb)	Low NLO c.s. (pb)
80	1.0 ± 0.2	0.44 ± 0.06	2.9	36.0
100	3.4 ± 0.6	0.44 ± 0.06	0.80	10.7
120	8.8 ± 1.4	0.44 ± 0.06	0.30	3.81
140	14.4 ± 2.1	0.44 ± 0.06	0.18	1.54
160	20.9 ± 3.0	0.44 ± 0.06	0.13	0.68
180	27.6 ± 3.8	0.44 ± 0.06	0.094	0.32
200	33.2 ± 4.0	0.44 ± 0.06	0.076	0.16
220	36.1 ± 4.4	0.44 ± 0.06	0.070	0.080

TABLE XV. Efficiency, background, upper limit on the leptoquark production cross section, and comparison with the NLO cross section [16] for $\beta = 1$ as a function of the leptoquark mass for the $eejj$ channel.

Mass (GeV)	Efficiency (%)	Background (Events)	95% C.L. c.s upper limit (pb)	Low NLO c.s. pb
50	$0.446 \pm 0.096 + 0.001 - 0.047$	3.49 ± 1.17	328	406
60	$1.11 \pm 0.15 + 0.05 - 0.06$	3.49 ± 1.17	77.0	162
80	$2.15 \pm 0.20 + 0.12 - 0.08$	3.49 ± 1.17	37.7	36.0
100	$3.90 \pm 0.27 + 0.12 - 0.13$	3.49 ± 1.17	21.0	10.7
120	$4.62 \pm 0.30 + 0.02 - 0.10$	3.49 ± 1.17	17.6	3.81
140	$6.07 \pm 0.34 + 0.02 - 0.04$	3.49 ± 1.17	13.2	1.54
160	$6.15 \pm 0.34 + 0.04 - 0.03$	3.49 ± 1.17	13.0	0.68
200	$6.36 \pm 0.35 + 0.04 - 0.06$	3.49 ± 1.17	12.6	0.16

TABLE XVI. Efficiency, background, upper limit on the leptoquark production cross section, and comparison with the NLO cross section [16] for $\beta = 0$ as a function of the leptoquark mass for the $\nu\nu jj$ channel.

Mass (GeV)	Efficiency (%)	Excluded β region (pb)
45†	0.3 ± 0.0	$[0.05, 0.95]$
60	1.2 ± 0.1	$[0.06, 0.94]$
80	3.3 ± 0.3	$[0.09, 0.91]$
100	7.1 ± 0.7	$[0.16, 0.84]$
120	11 ± 1	$[0.42, 0.58]$

TABLE XVII. Efficiency and excluded β regions as a function of the leptoquark mass for the unoptimized $e\nu jj$ channel analysis based on 14 event base sample.

M_{ej1}	M_{ej2}	$M_T^{\nu j1}$	$M_T^{\nu j2}$
0.96	0.945	0.885	0.78

TABLE XVIII. Mass fitter coefficients

†Obtained by scaling down the cuts applied to LQ60 sample

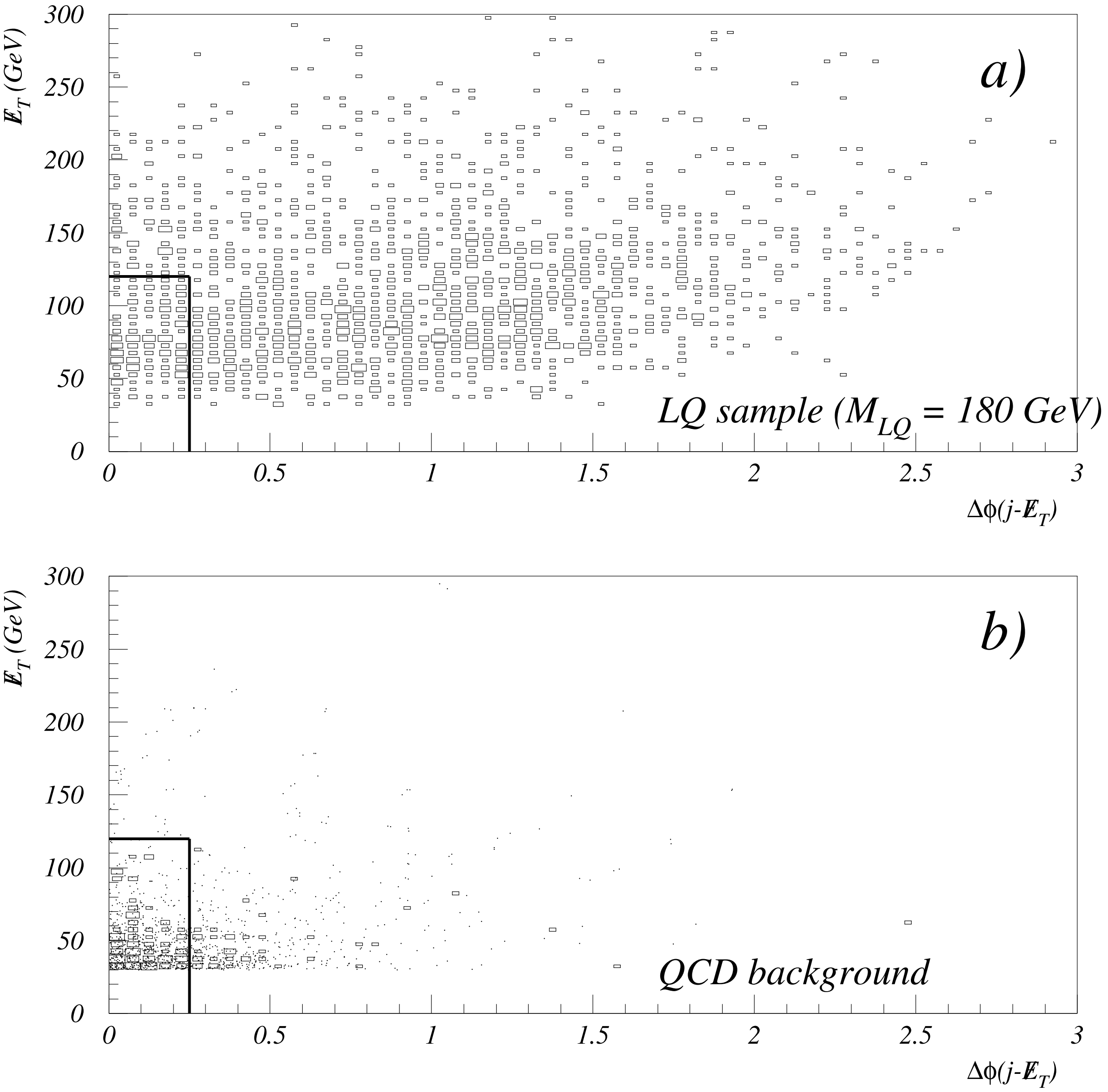

FIG. 1. $\not{E}_T$ acollinearity cut effect on the (a) leptoquark signal with $M_{LQ} = 180$ GeV and (b) QCD background (dots – before the $M_T^{e\nu}$-cut; boxes – thereafter. Acollinearity cut is shown with a solid line.

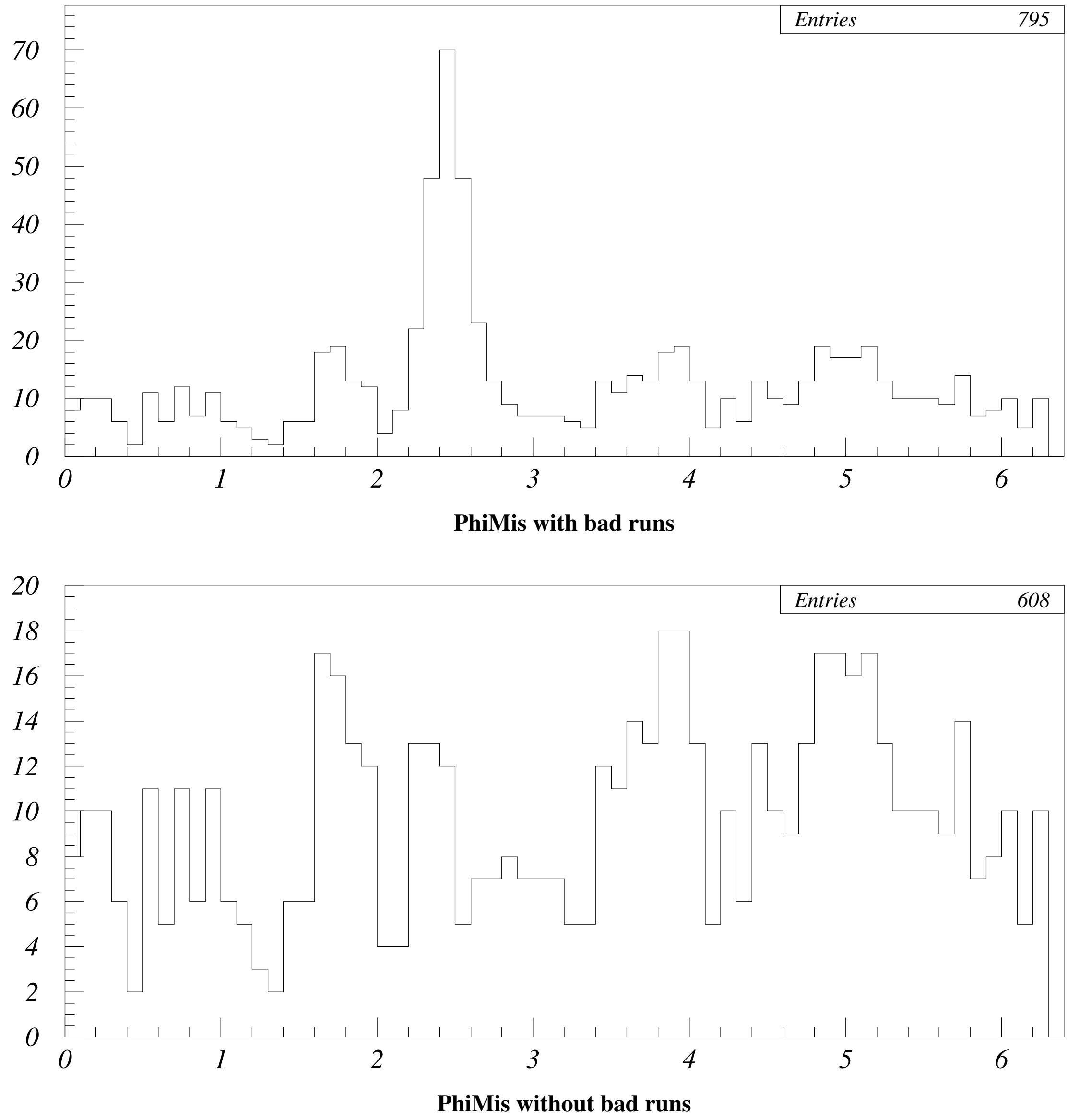

FIG. 2. $\not{E}_T$ azimuthal direction for the QCD sample. a) before the additional bad run removal; b) thereafter.

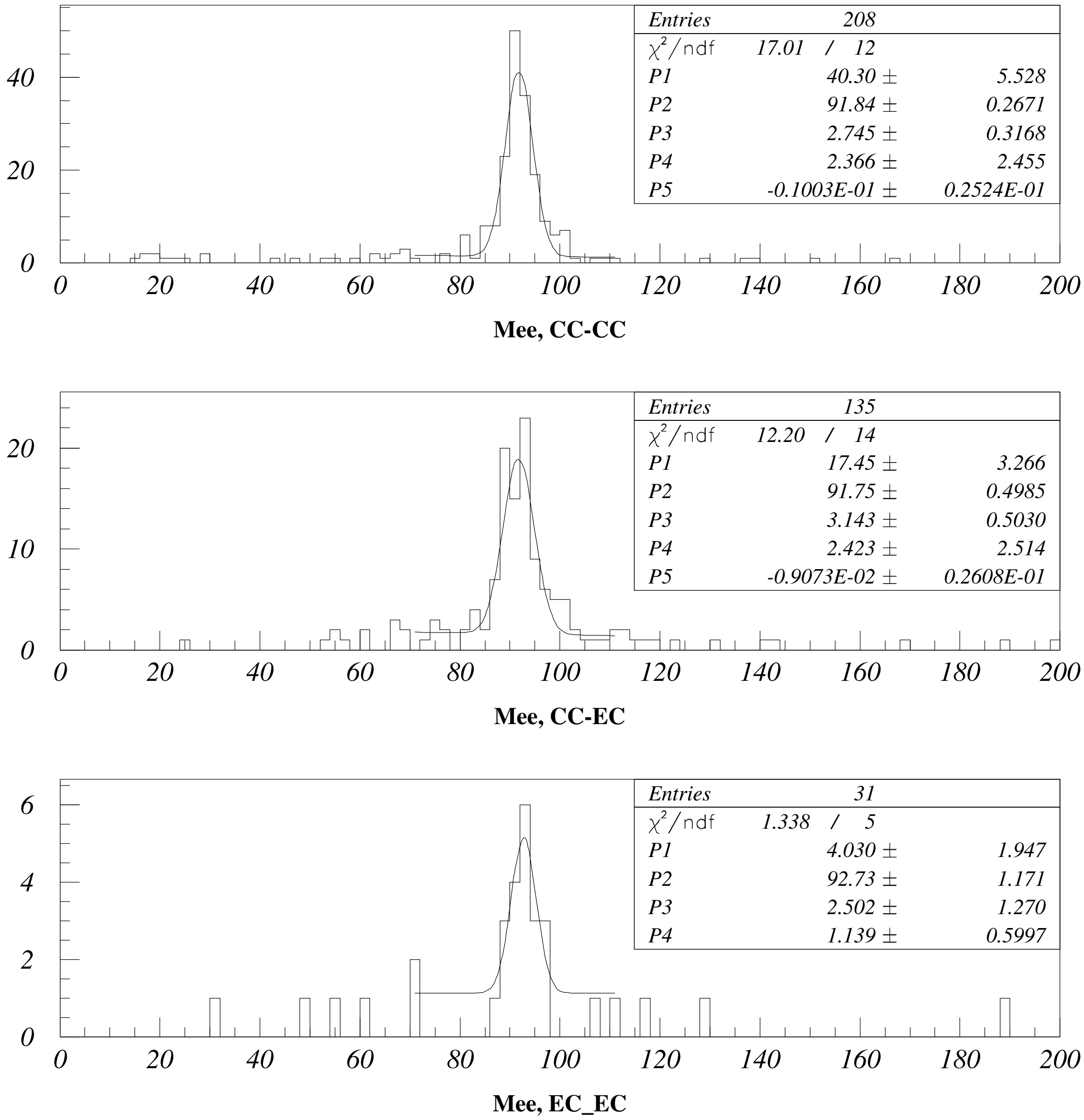

FIG. 3. Z-peak in the $Z + 2j$ data events for three topological configurations of the dielectron pair: a) CC-CC; b) CC-EC; c) EC-EC. Peak was fitted with a sum of a Gaussian and a second order polynomial.

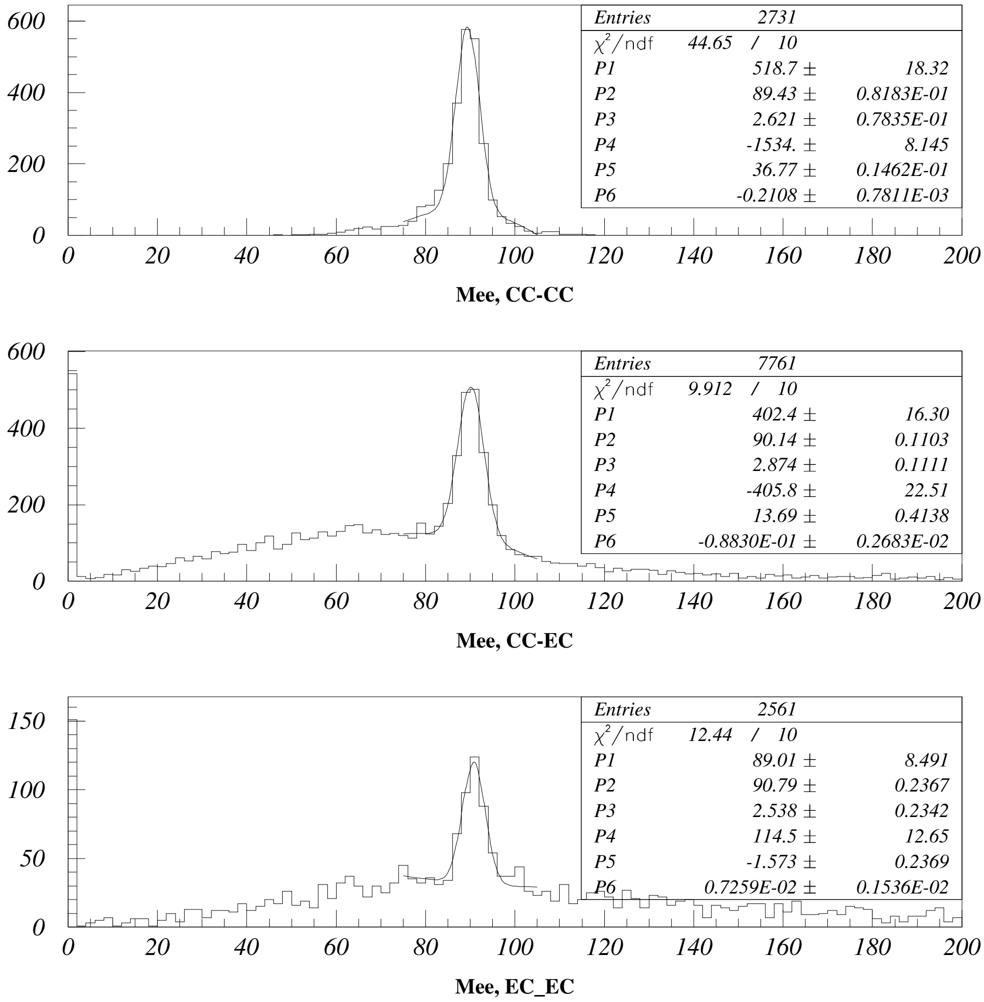

FIG. 4. Z-peak in the $Z + 2j$ Monte Carlo events for three topological configurations of the dielectron pair: a) CC-CC; b) CC-EC; c) EC-EC. Peak was fitted with a sum of a Gaussian and a second order polynomial.

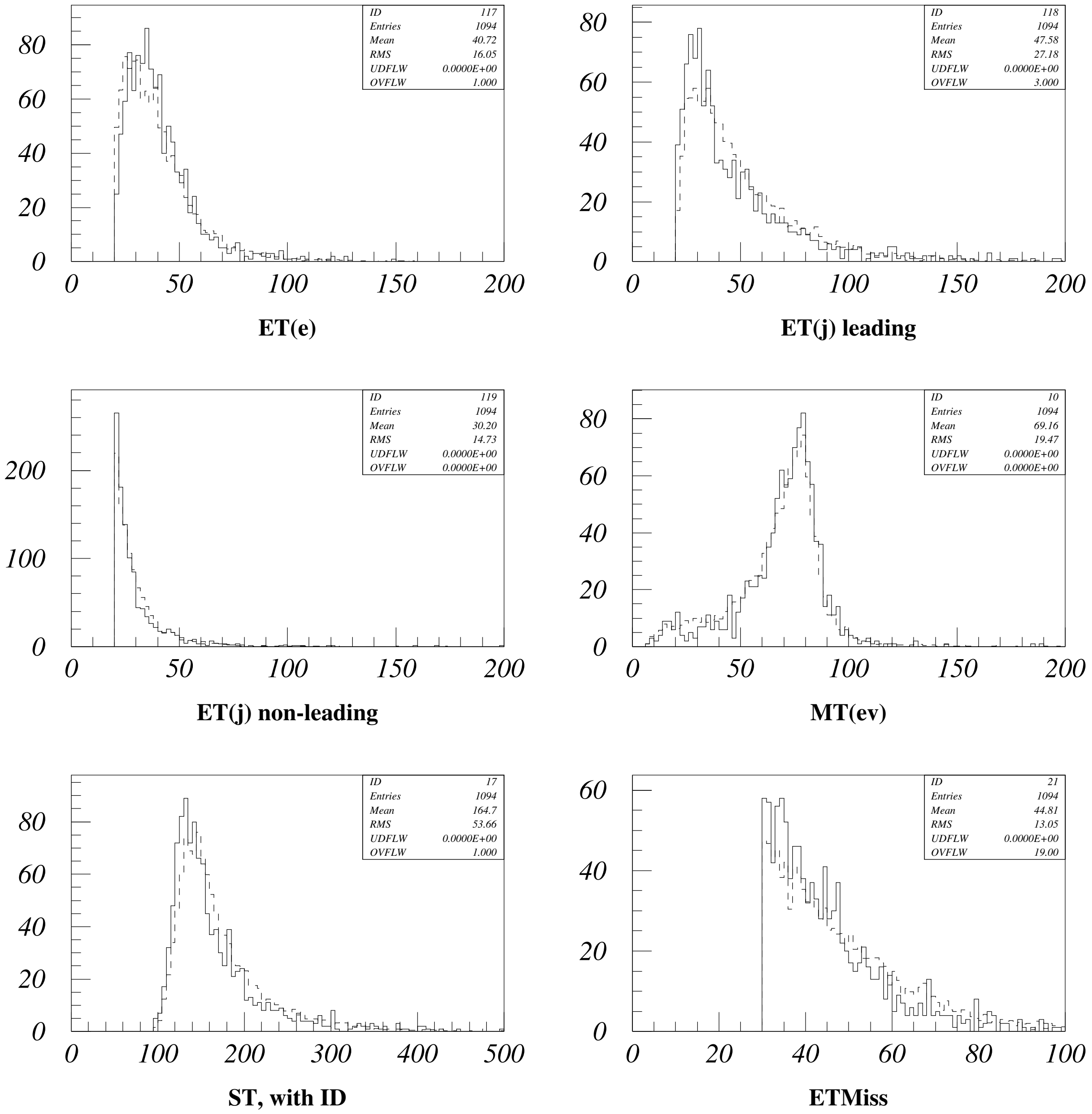

FIG. 5. Comparison of the event parameter for the data (solid) and predicted background (dashed). Row-wise top to bottom: E_T^e, E_T^{j1}, E_T^{j2}, $M_T^{e\nu}$, S_T^{12}, and $\not{E}_T$. Basic cuts except for the $M_T^{e\nu}$ cut were applied to both data and the background samples.

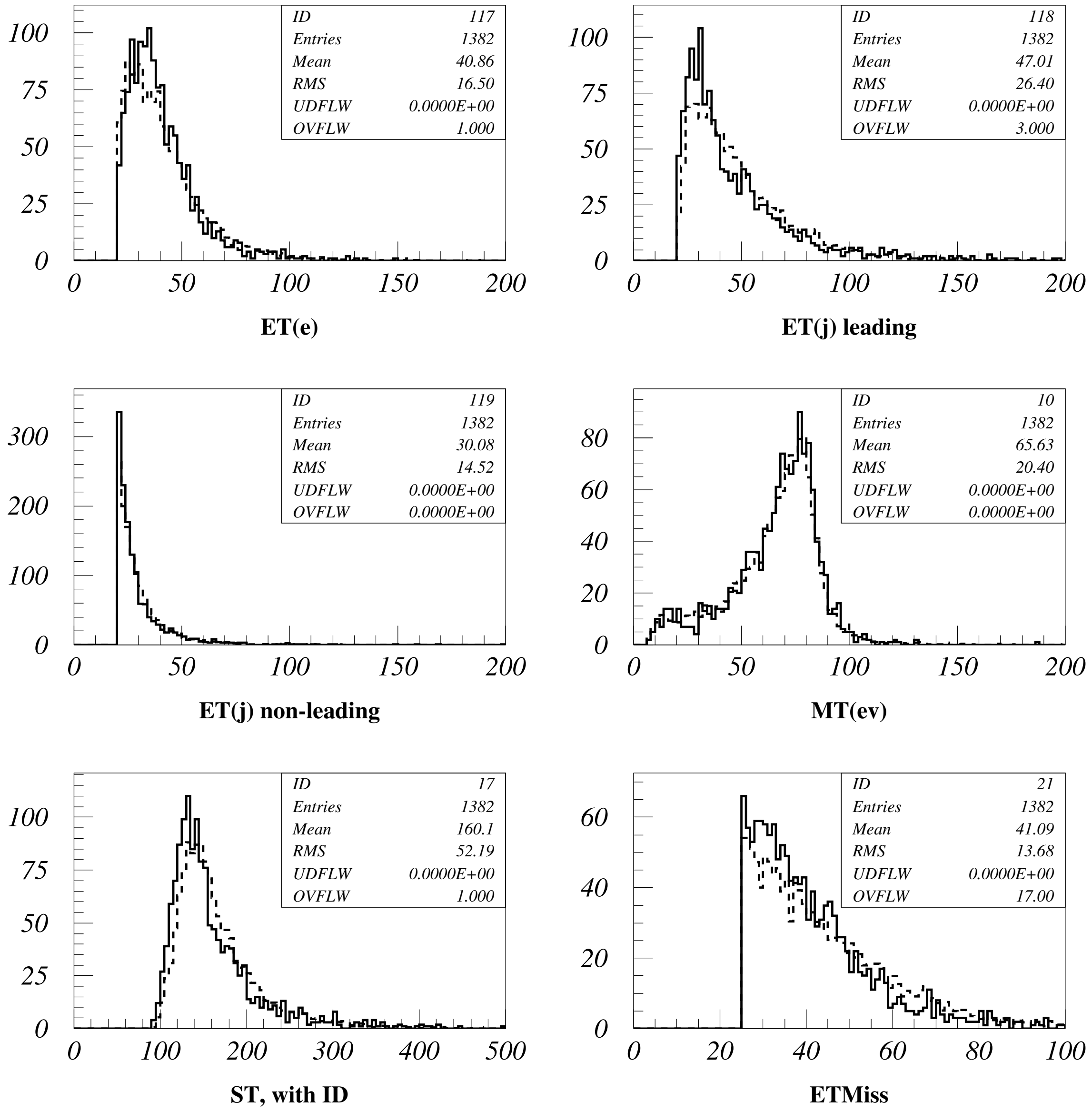

FIG. 6. Comparison of the event parameter for the data (solid) and predicted background (dashed). Row-wise top to bottom: E_T^e, E_T^{j1}, $E_T^{j2}, M_T^{e\nu}, S_T^{12}$, and $\not{E}_T$. $\not{E}_T$ $>$ 25 GeV cut was used for both data and the backgrounds.

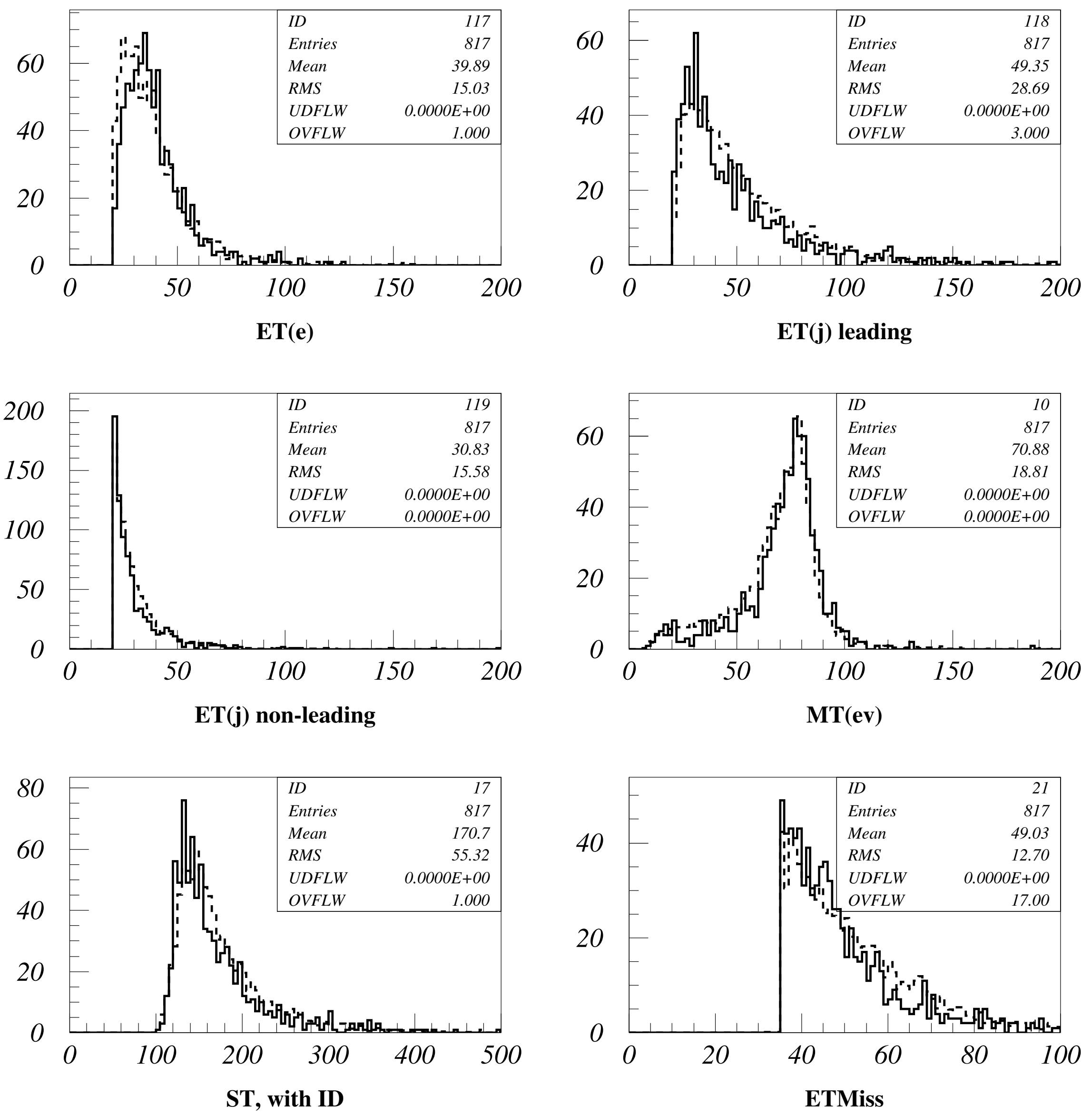

FIG. 7. Comparison of the event parameter for the data (solid) and predicted background (dashed). Row-wise top to bottom: E_T^e, E_T^{j1}, $E_T^{j2}, M_T^{e\nu}, S_T^{12}$, and $\not{E}_T$. $\not{E}_T$ $>$ 35 GeV cut was used for both data and the backgrounds.

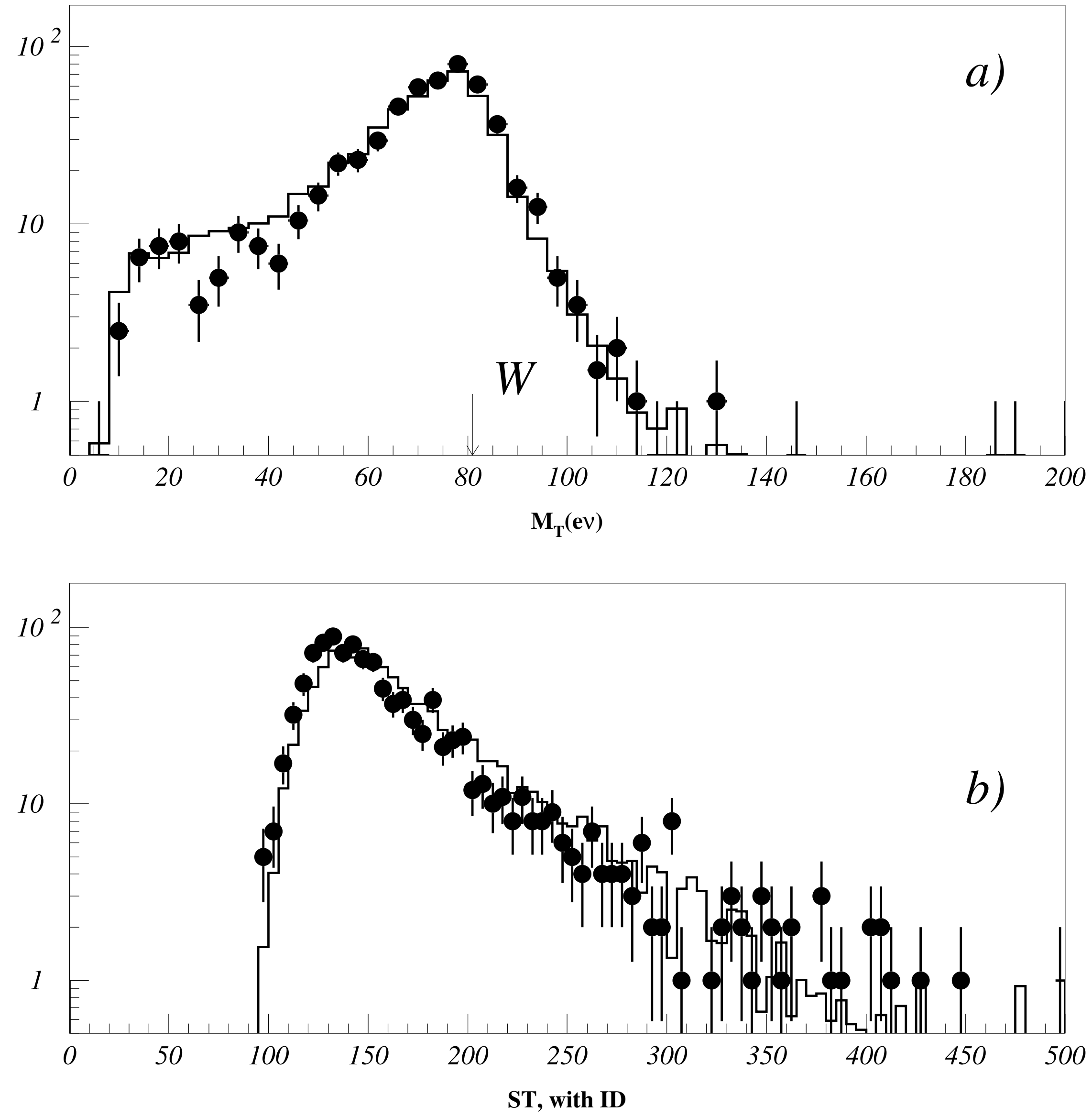

FIG. 8. Comparison of the (a) $M_T^{e\nu}$ and (b) S_T^{12} distributions for the data (points with error bars) and $W + 2j$ MC (solid histogram).

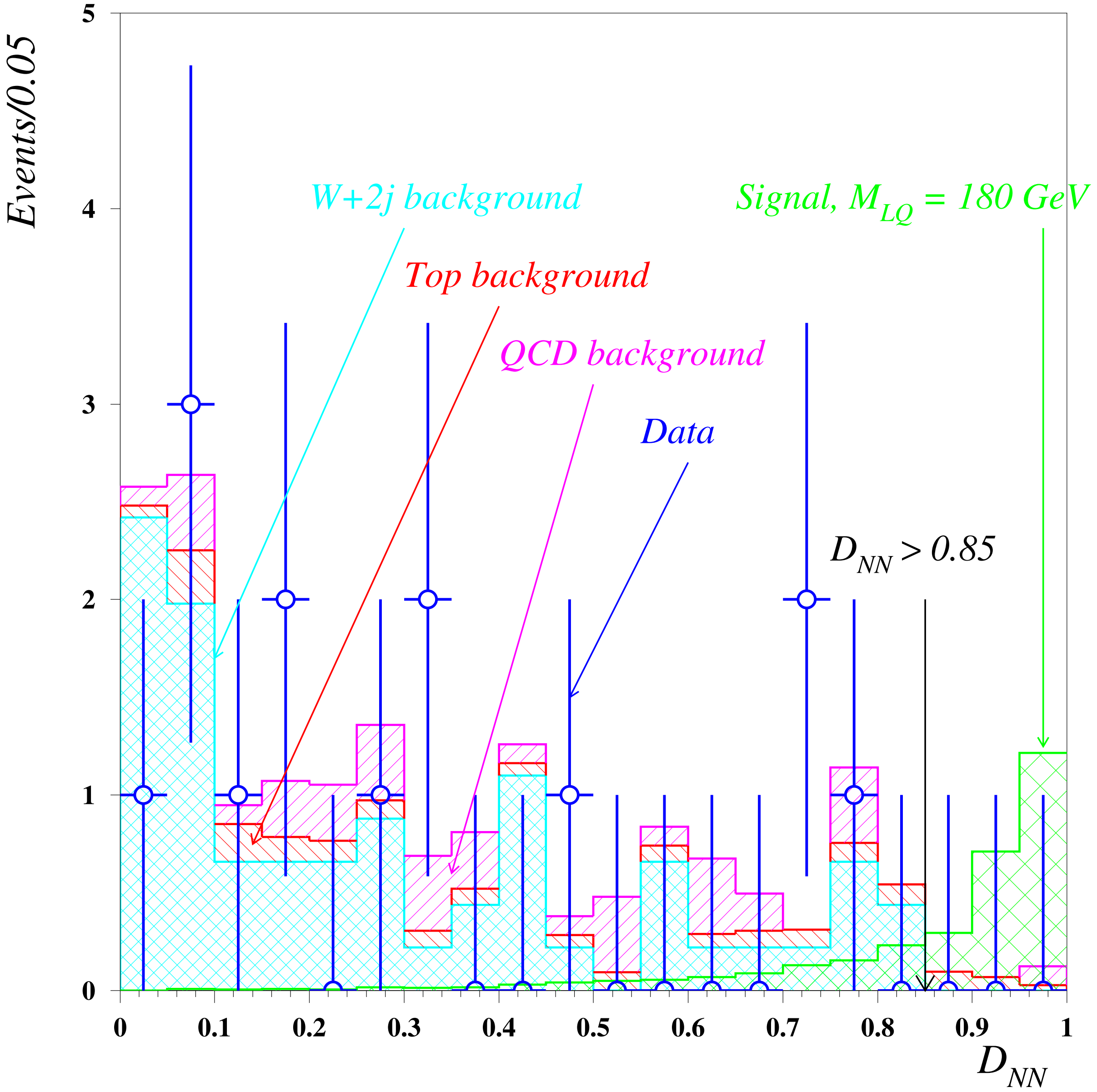

FIG. 9. Predicted background, signal and number of data events as a function of the $\mathcal{D}_{NN}$ cut.

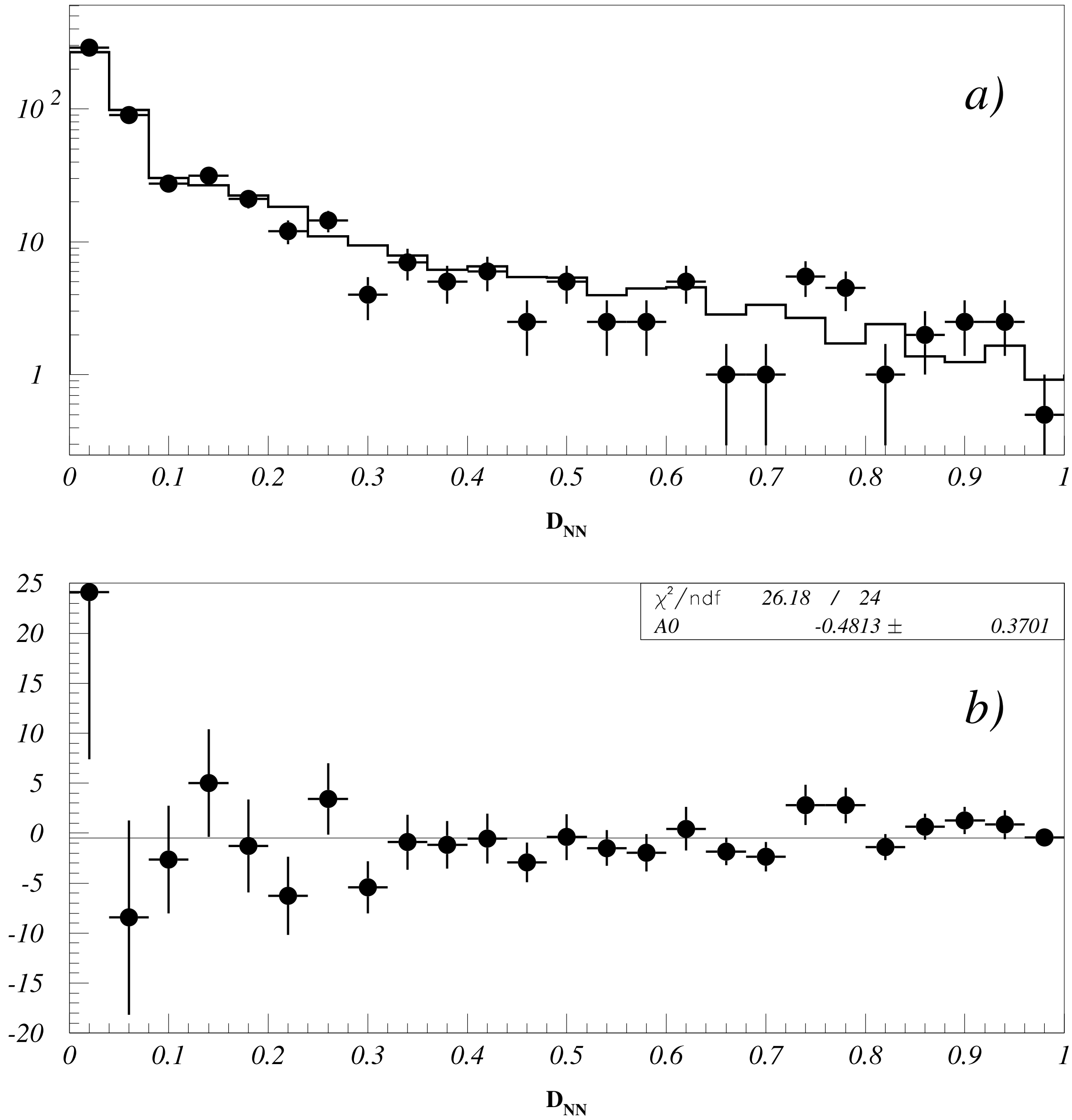

FIG. 10. Comparison of the $\mathcal{D}_{NN}$ distribution in the loose data set with that expected for the background. a) Points – data; histogram – background prediction. b) Histogram – data minus background prediction; line – fit with a constant to illustrate proper normalization and good χ^2.

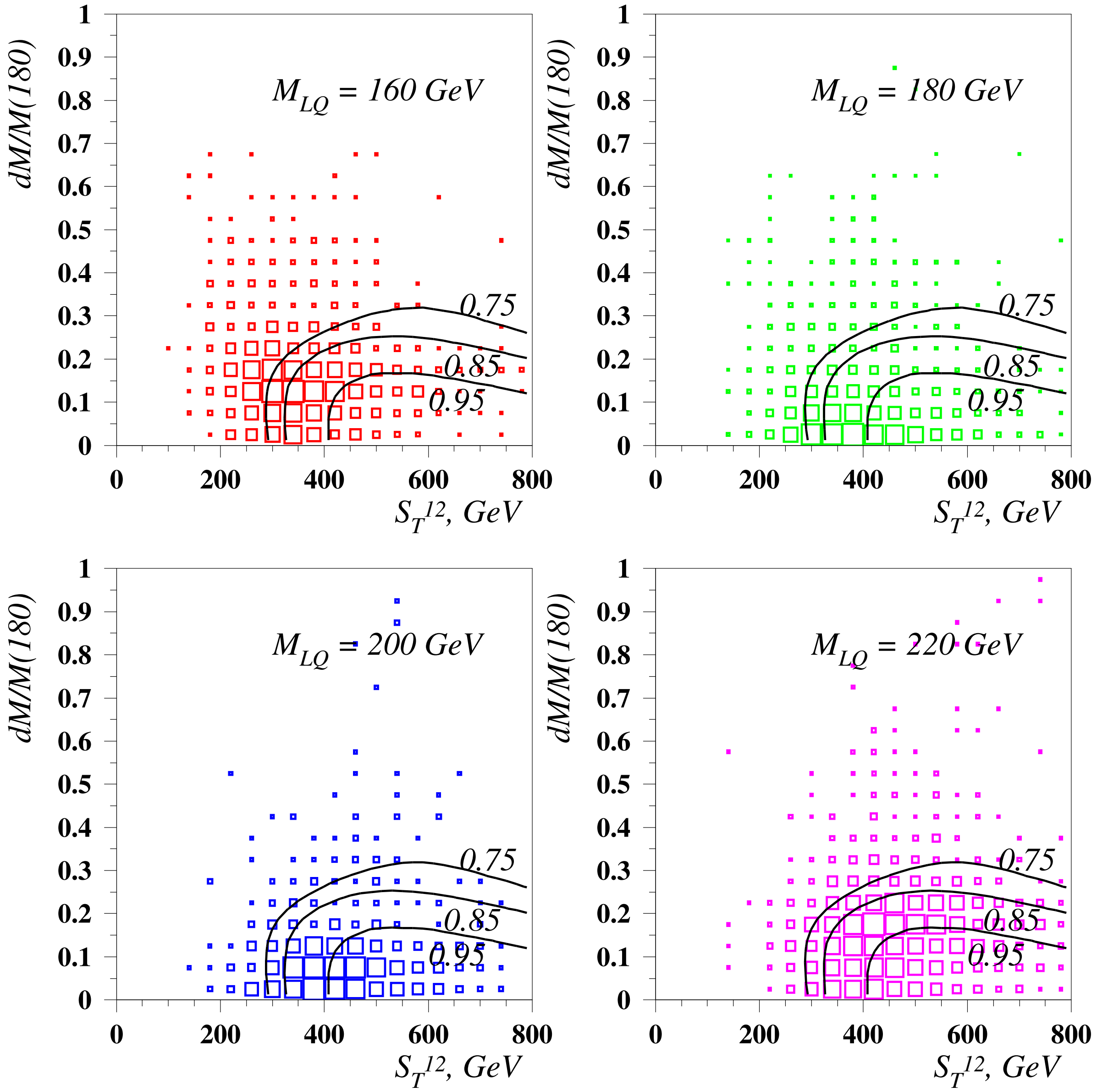

FIG. 11. NN training on the signal. Only loose cuts applied. Curves show neural net equidiscriminant contours for $\mathcal{D}_{NN}$ = 0.95, 0.85, and 0.75. LQ masses: (a) 160 GeV; (b) 180 GeV; (c) 200 GeV; (d) 220 GeV.

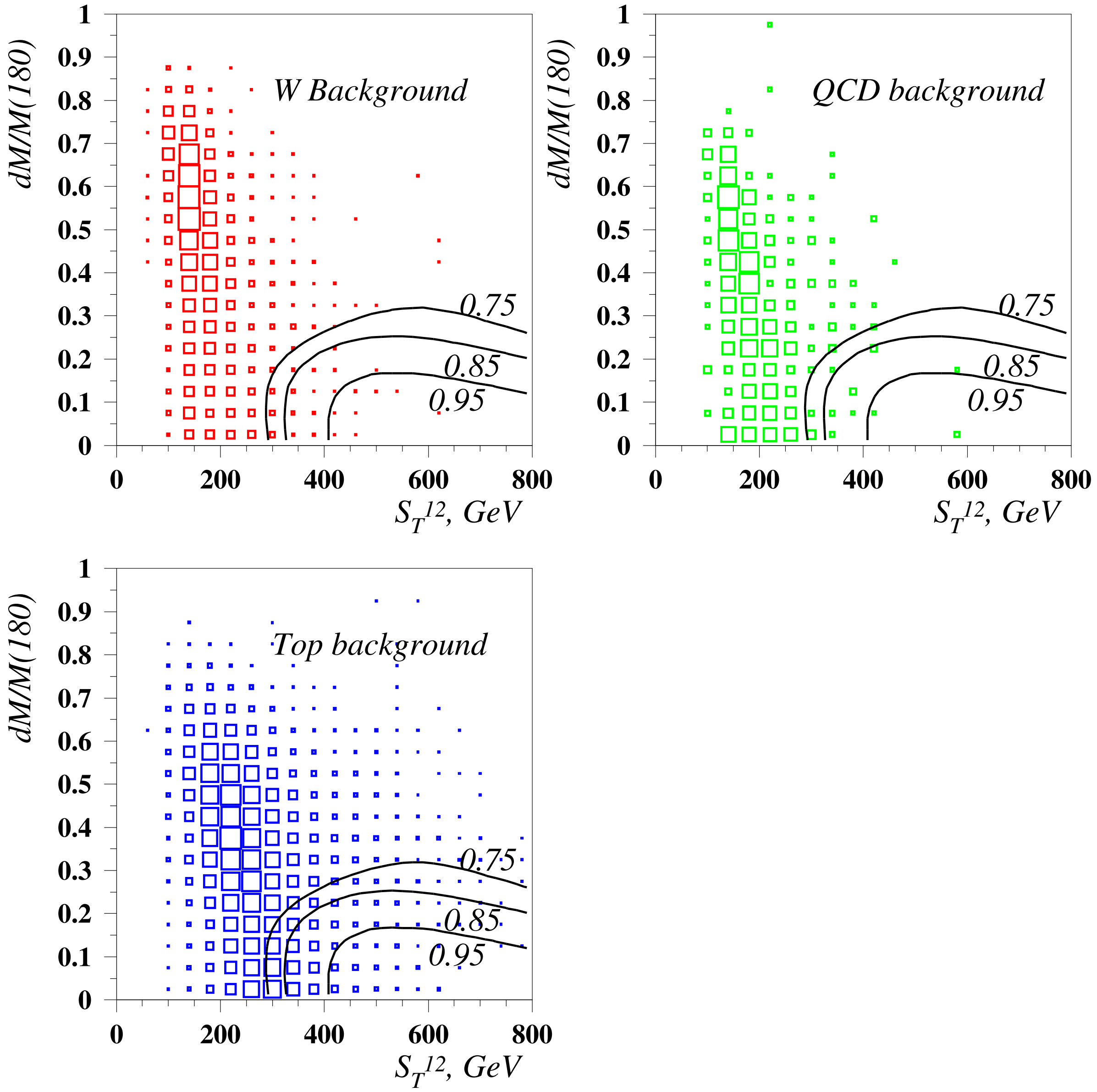

FIG. 12. NN training on the background. Only loose cuts applied. Curves show neural net equidiscriminant contours for $\mathcal{D}_{NN}$ = 0.95, 0.85, and 0.75. (a) $W + 2j$; (b) QCD; (c) top.

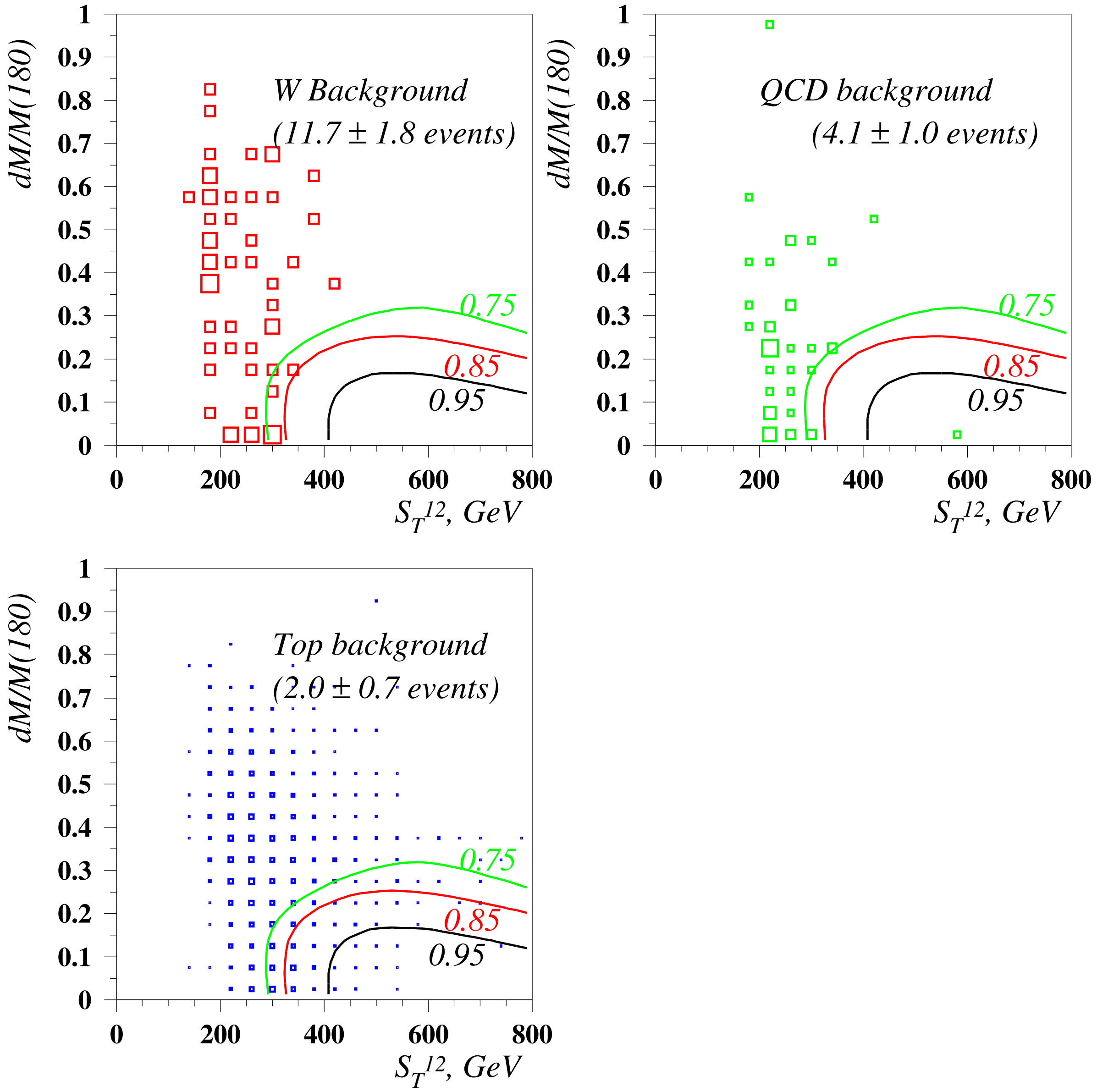

FIG. 13. NN rejection of the background. Basic cuts are applied. Curves show neural net equidiscriminant contours for $\mathcal{D}_{NN}$ = 0.95, 0.85, and 0.75. (a) $W + 2j$; (b) QCD; (c) top.

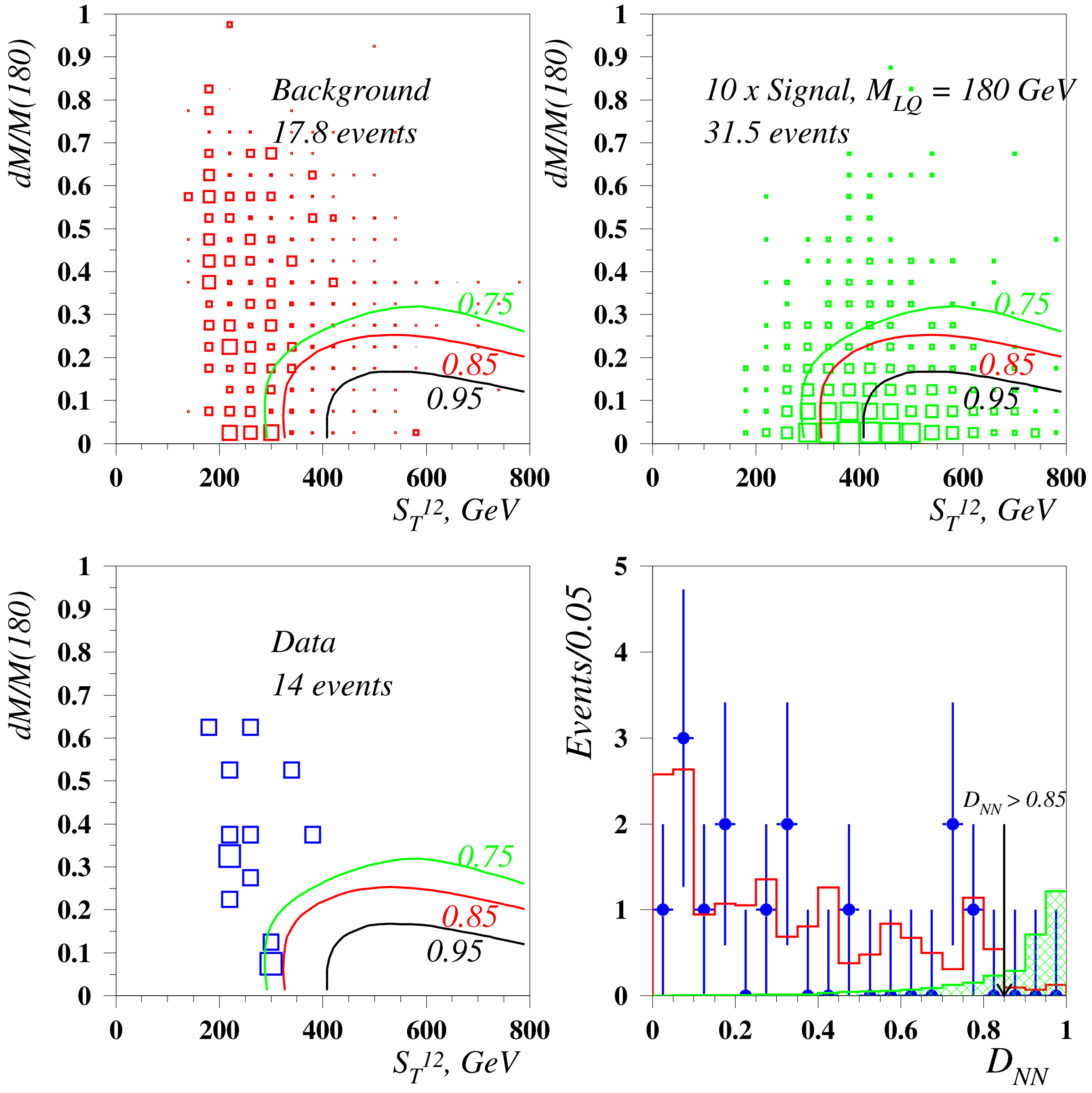

FIG. 14. (a) NN discriminant for signal, background and data. (b)-(d) S_T^{12} vs. $\Delta M/M(180)$ for signal, sum of the backgrounds and data. Curves show neural net equidiscriminant contours for $\mathcal{D}_{NN}$ = 0.95, 0.85, and 0.75.

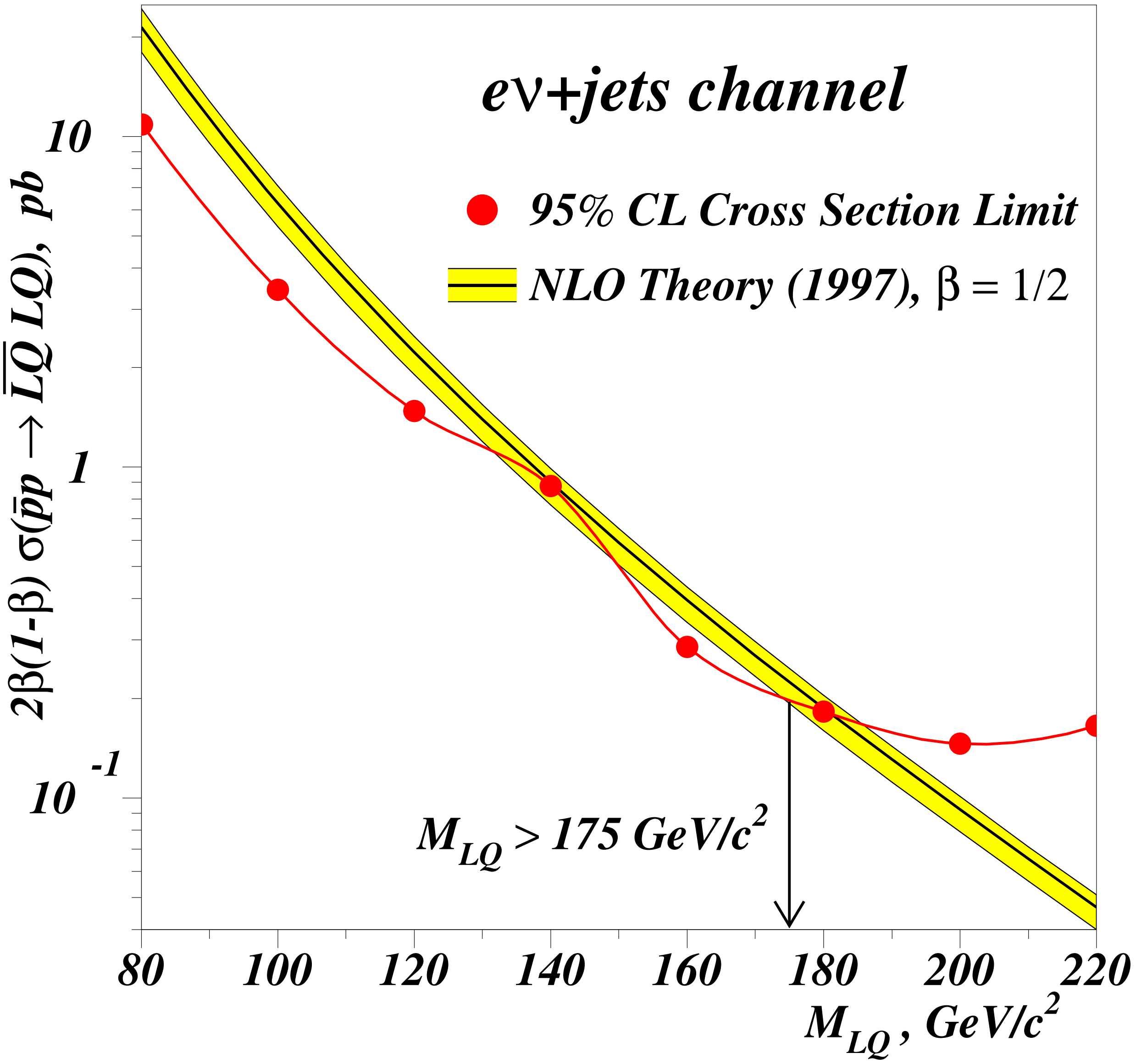

FIG. 15. 95% CL cross section limit based on $dM/M(180)$ network only and its comparison with the NLO theoretical predictions as a function of the LQ mass.

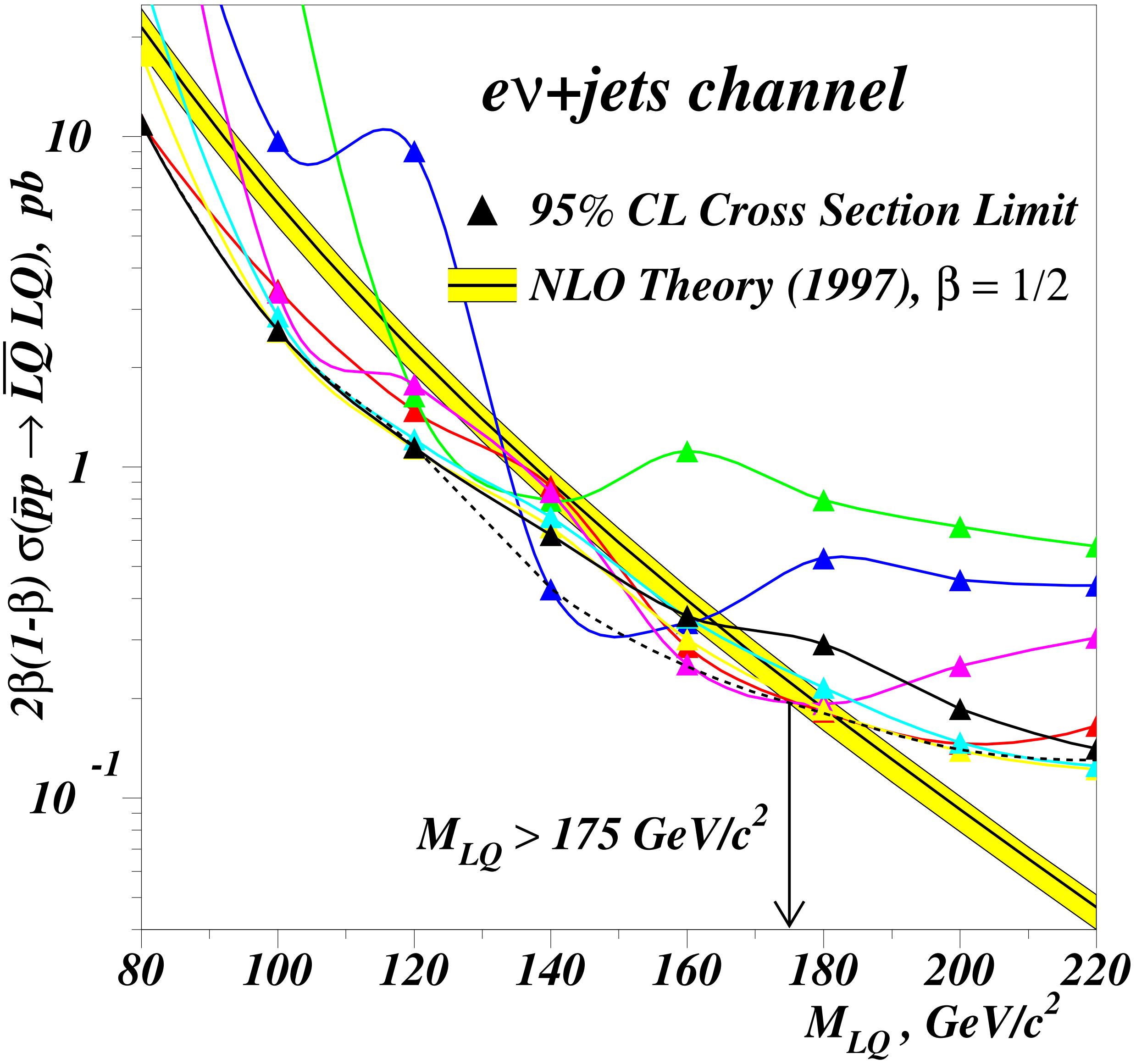

FIG. 16. 95% CL cross section limit and NLO theoretical prediction vs. LQ mass for all six neural nets used in the analysis. Dashed black line shows an envelope limit which is the final 95% CL cross section limit obtained in this analysis.

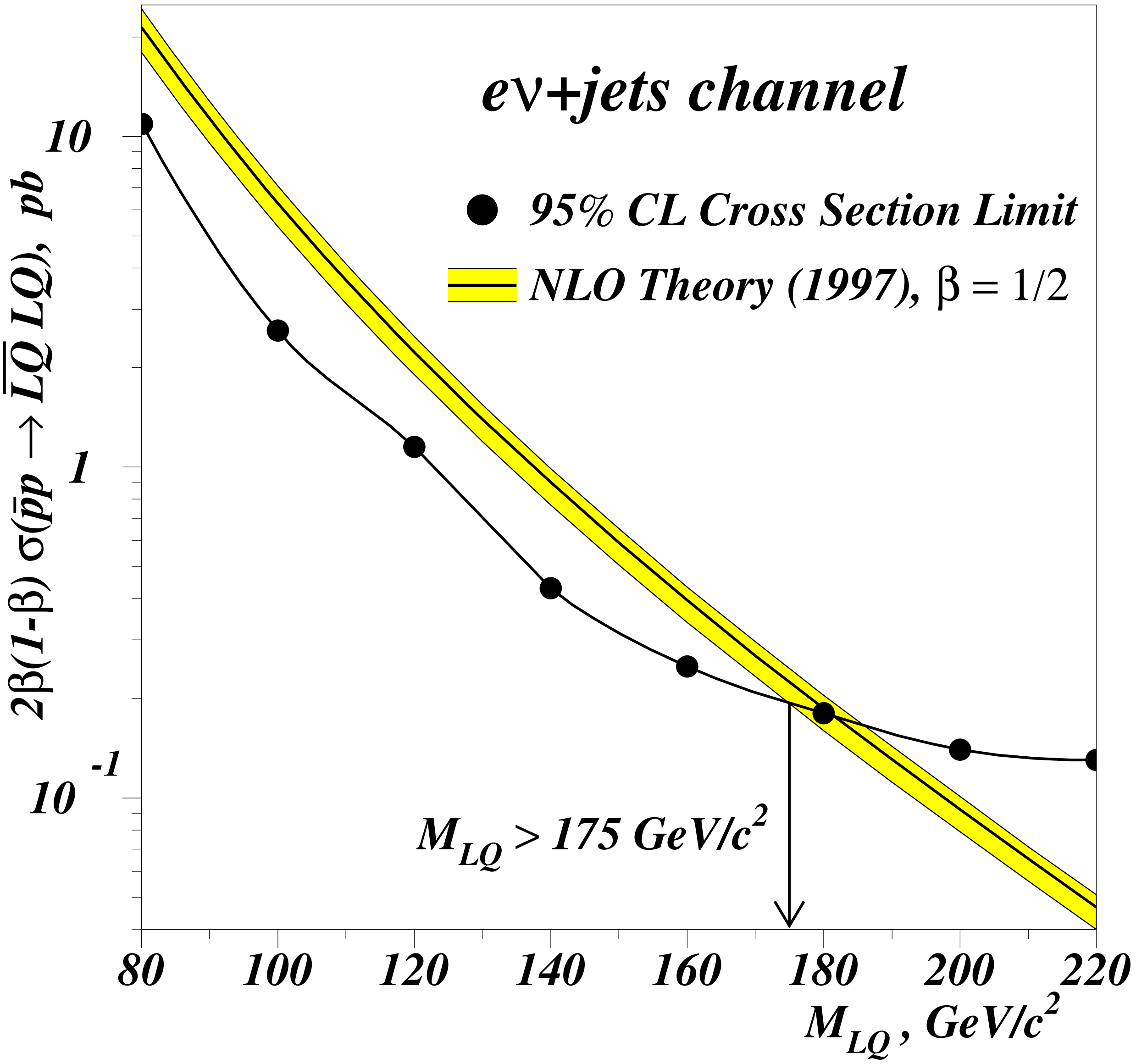

FIG. 17. Final 95% CL cross section limit from the $e\nu jj$ analysis and NLO theoretical prediction vs. LQ mass.

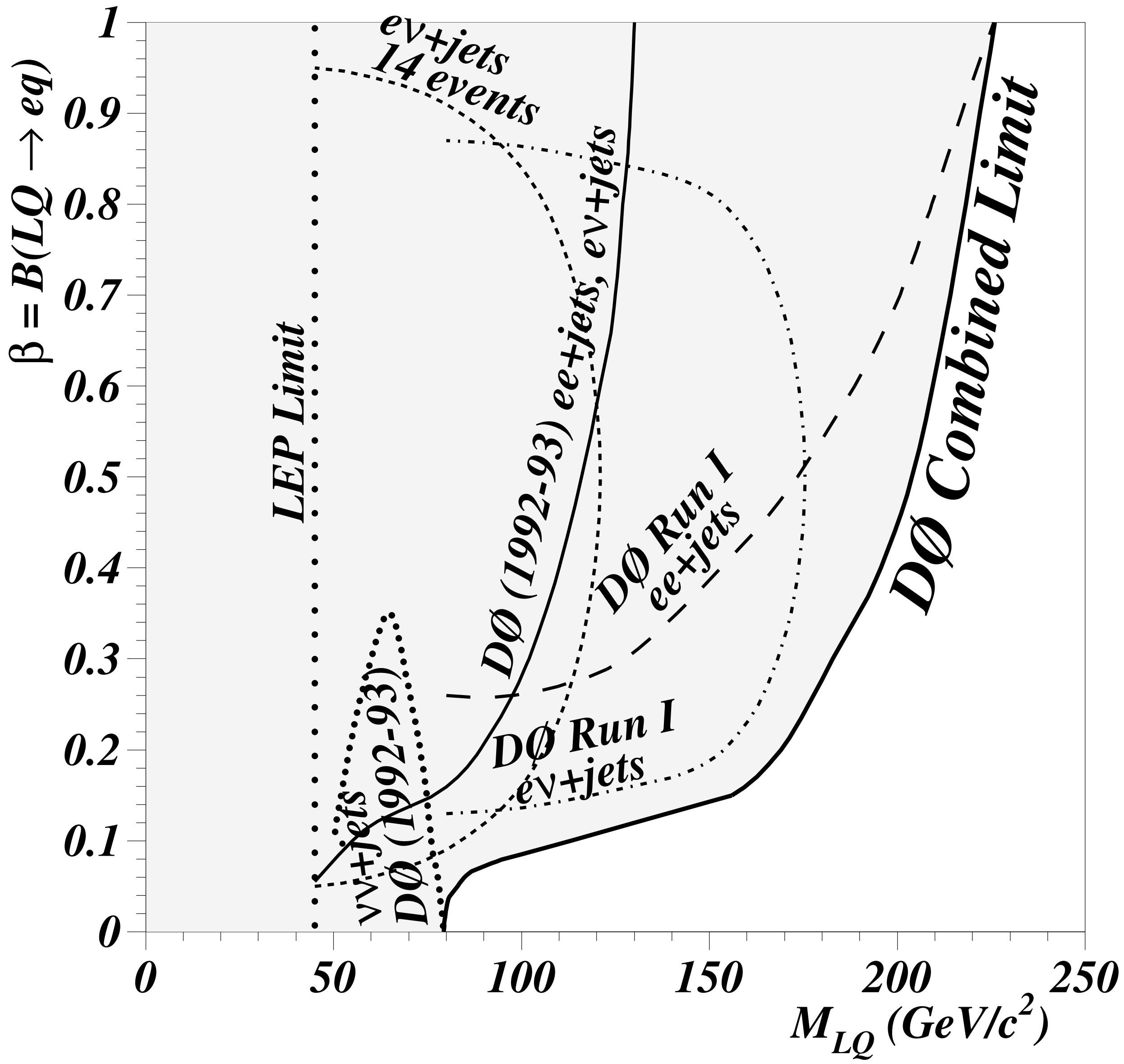

FIG. 18. 95% CL lower mass limit on the fist generation scalar leptoquark from combined $eejj$, $e\nu jj$, and $\nu\nu jj$ data as a function of branching ratio β.

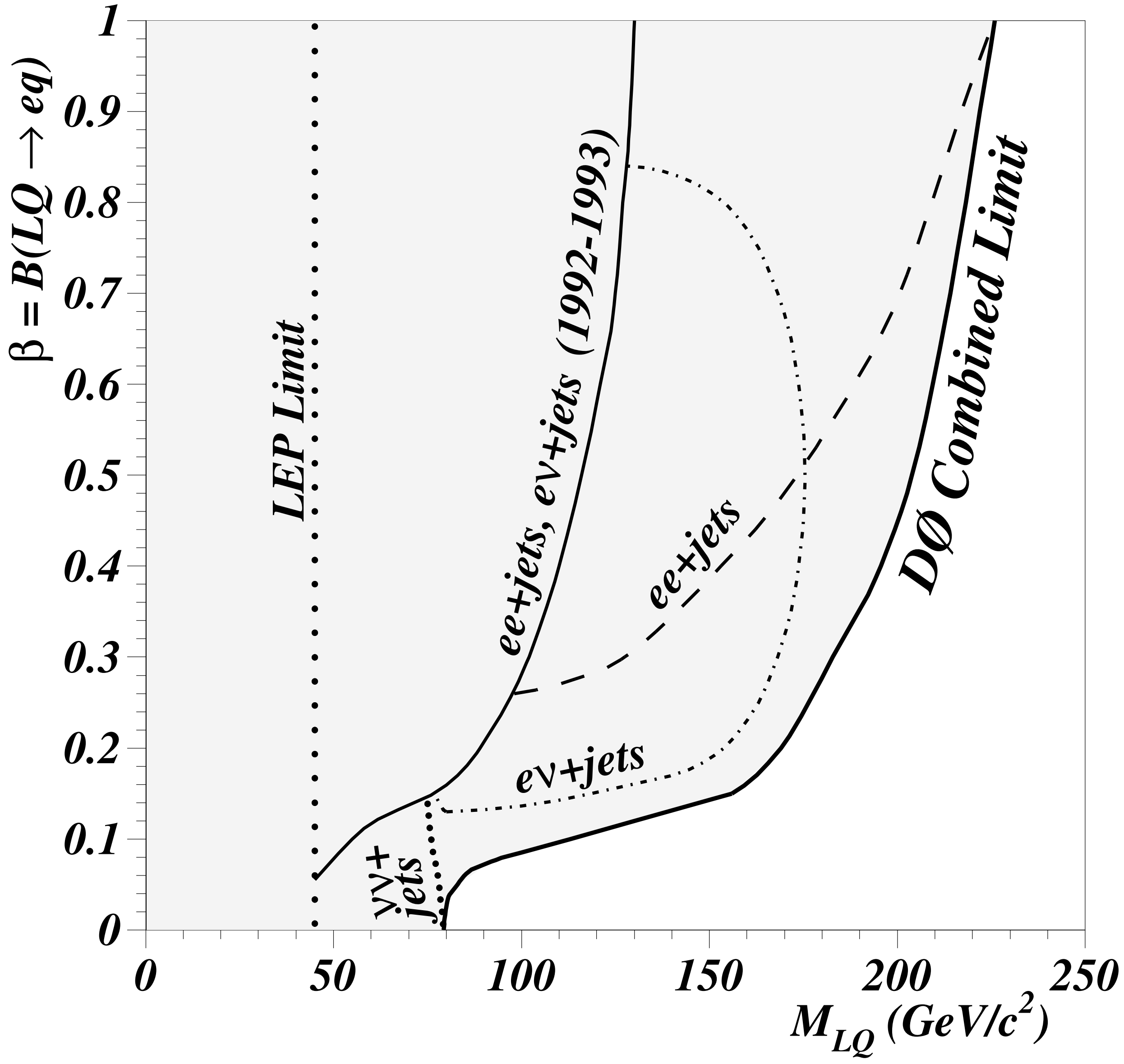

FIG. 19. 95% CL lower mass limit on the fist generation scalar leptoquark from combined $eejj$, $e\nu jj$, and $\nu\nu jj$ data as a function of branching ratio β.

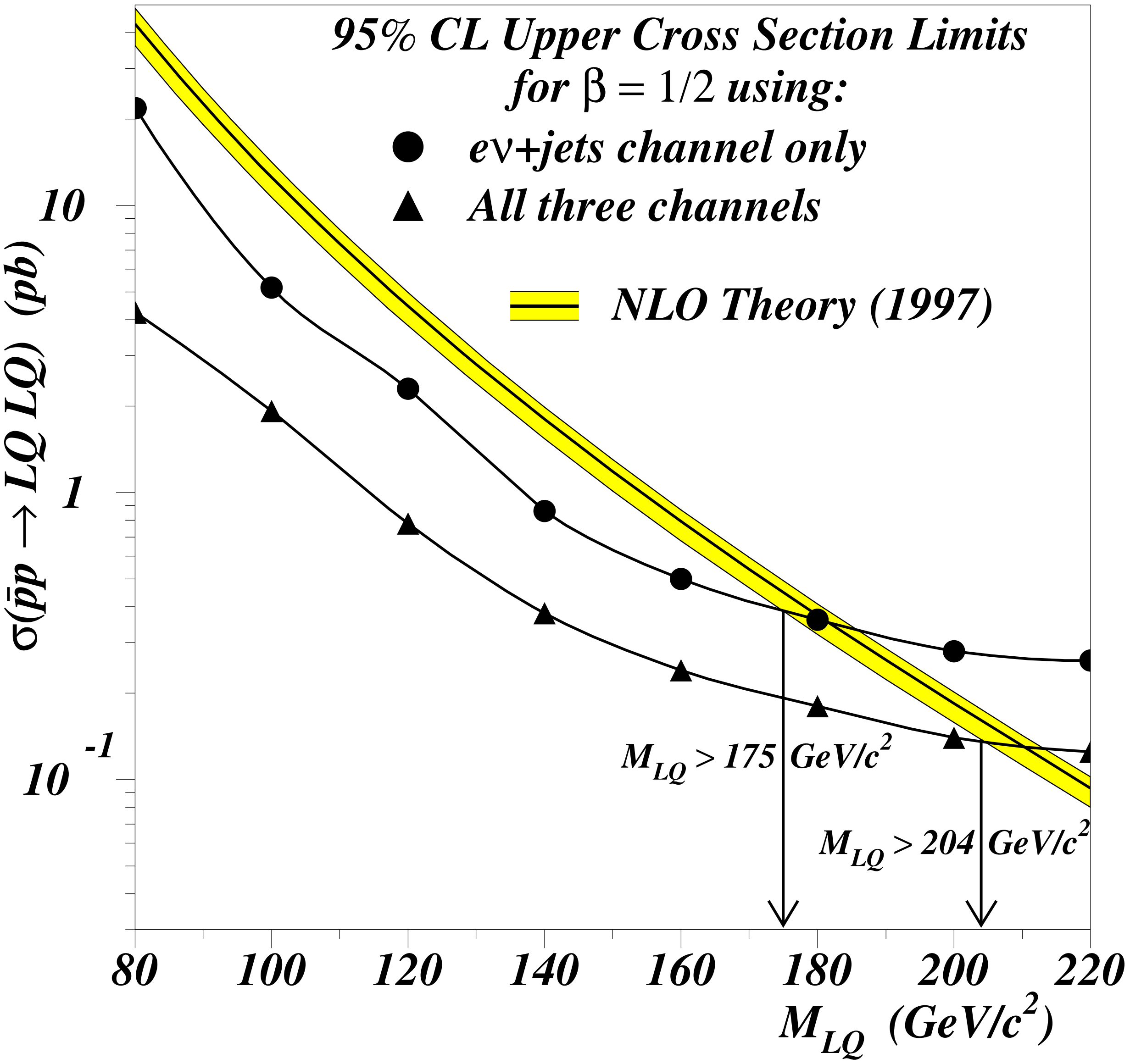

FIG. 20. Upper 95% CL cross section limit from the $e\nu jj$ and combined analyses for $\beta = 1/2$ as well as NLO theoretical prediction vs. LQ mass.